THE INFLUENCE OF HALL CURRENTS ON UNSTEADY-MHD HEAT TRANSFER FLOWIN A CONDUCTING CHANNEL CONTAINING TWO IONIZED FLUIDS

V. Gowri Sankara Rao

Dept. of Mathematics, St. Joseph's College for Women (A), Visakhapatnam, INDIA

T. Linga Raju[*]

Department of Engineering Mathematics, AUCE (A), Andhra University, Visakhapatnam, INDIA
E-mail: prof.tlraju@andhrauniversity.edu.in, tlraju45@yahoo.com

We delve into the effects of hall currents on the dynamics of unsteady magnetohydrodynamic flow and heat transfer within a two-fluid system of ionized gases confined within a horizontal channel bounded by parallel conducting plates. Employing a regular perturbation technique, we solve the governing partial differential equations to unveil the distributions of velocity and temperature, alongside profiles depicting heat transfer coefficients. Through a systematic parametric analysis, we explore the interplay among variables such as the Hartmann number, Hall parameter, and ratios involving viscosities, heights, electrical conductivities, and thermal conductivities. The results highlight the profound influence of these parameters on the dynamics of unsteady magnetohydrodynamic (MHD) heat transfer within a flow regime characterized by a dual-ionized fluid. This influence is particularly pronounced when the lateral plates of the channel are conductive. Significantly, elevated Hartmann numbers and Hall parameters are associated with augmented heat transfer coefficients at both plates, holding other variables constant.

Key words: Hall effect, magnetohydrodynamic (MHD) heat transfer, plasma dynamics, immiscible flow, conductive porous plates, regular perturbation method.

1. Introduction

Recent technological progress has sparked a keen interest in exploring studies related to magnetohydrodynamic (MHD) multi-fluid or immiscible fluid flow. This enthusiasm is stimulated by the widespread applications of such studies across diverse specialized fields. Notably, the conceptual design of fusion reactors, liquid metal MHD power generators, MHD accelerators, and electromagnetic pumps necessitates a thorough understanding of heat transfer and thermo-hydraulic mechanisms within two-phase or two-fluid flow models influenced by an applied magnetic field. The adoption of two-fluid flow models has proven to be particularly advantageous in enhancing heat transfer under specific conditions. In the context of transportation and the extraction of oil products in geothermal regions, the implementation of a two-phase or two-fluid flow model, especially in an electromagnetic pump, leads to improved flow rates. Furthermore, it reduces the power required for oil pumping through pipelines, as demonstrated by the effective incorporation of water, as observed in Shail [1].

Recognizing that fluid flows, whether Newtonian or non-Newtonian are generally characterized by an unsteady or transient nature, this property poses significant challenges, particularly in practical scenarios involving immiscible fluids. Many issues in industries such as petroleum, geophysics, plasma physics, and magneto-fluid dynamics revolve around multi-fluid flow situations. Considering both immiscible fluids as electrically conducting, with one having high electrical conductivity compared to the other, proves beneficial in minimizing power consumption during operations like pumping fluids in MHD pumps and flow meters. In

---

[*] To whom correspondence should be addressed

numerous engineering, technological, and industrial challenges, understanding the heat flow magnitude and the resulting temperature distribution patterns during unsteady motion in various geometries is crucial. Oscillatory flows are commonly employed to enhance heat transfer rates in various industrial processes. Cowling [2] emphasized that in ionized gas working fluids with low density or strong magnetic fields, the influence of Hall currents becomes significant, leading to the unavoidable Hall effect.

Hence, there is a significant requirement to investigate the influence of Hall currents on the dynamics of unsteady magnetohydrodynamic two-fluid flow. Hall currents play a crucial role in various astrophysical and geophysical scenarios, as well as in plasma flows found in MHD power generators, plasma jets, Hall accelerators, and similar applications. Numerous model studies have been conducted by researchers over several decades to examine the impact of Hall currents on MHD problems involving single fluid flow systems [3-22]. While there exists a substantial body of literature on MHD two-phase/two-fluid flow problems due to their extensive applications across various domains [23-39], most of these studies assume steady-state conditions in their analyses. However, practical applications often involve understanding the effect of external body forces on the motion of electrically conducting fluids in two-dimensional time-dependent situations. Therefore, further research is needed to explore how unsteady MHD two-fluid flow dynamics are affected by the presence of Hall currents. This investigation will contribute to our understanding of complex phenomena and enable us to develop more accurate models for real-world scenarios involving time-dependent fluid motion influenced by external forces.

Despite the aforementioned studies, there is a limited body of research in the literature addressing magnetohydrodynamic two-fluid flow models with and without the Hall effect. Noteworthy among these studies are the works of Kalra *et al.* [40], who explored the impact of Hall current and resistivity on the stability of a gas-liquid system, and Hyun and Kennel [41], who discussed small amplitude waves in a hot relativistic two-fluid plasma. Sharma and Sharma [42] delved into MHD two-fluid flow and heat transfer through a horizontal channel, while Joseph *et al.* [43] examined unsteady MHD free convective flows of two immiscible fluids in a horizontal channel with heat and mass transfer. Sivakamini and Govindarajan [44] studied unsteady MHD flow of two immiscible fluids under chemical reaction in a horizontal channel, while Gireesha and Mahantesh [45] focused on studying Hall effects on dusty nanofluid two-phase transient flow past a stretching sheet. In more recent investigations, L. Raju conducted research on various aspects of MHD heat transfer in different fluid flow scenarios. For instance, L.Raju investigated MHD heat transfer in a two-ionized fluid flow between parallel plates with Hall currents [46,47]. L.Raju also collaborated with Gowri to study the effect of Hall current on unsteady MHD two-ionized fluid flow and heat transfer in non-conducting and conducting channels [48,49]. Furthermore, L.Raju worked with Valli to examine Hall currents influence on EMHD 2-layered plasma heat transfer flow via a channel of porous plates [50]. L. Raju, in collaboration with Venkat, explored rotating systems using a straight channel between non-conducting and conducting plates with Hall currents [51,52]. Furthermore, L. Raju and Satish examined slip regime MHD 2-liquid plasma heat transfer flow with Hall currents between parallel plates [53,54].

Previous explorations have primarily concentrated on steady flow conditions. Yet, prior studies have not delved into the realm of unsteady magnetohydrodynamic (MHD) two-fluid flow and heat transfer of ionized gases in a horizontal channel under the influence of a transverse magnetic field, incorporating Hall currents. This investigation aims to bridge this research gap by analyzing the influence of the Hall effect on the dynamics of fluctuating MHD two-fluid flow and heat transfer of ionized gases within a horizontal channel confined by two conducting plates and exposed to a transverse magnetic field. This theoretical endever carries practical significance in various engineering domains, such as chemical, petroleum, and especially geothermal systems. The findings may inform the design of MHD power generators, pumps, flow meters, Hall accelerators, and plasma jets. Moreover, they could enhance cooling processes in nuclear reactors and other engineering applications.

2. Derivation and mathematical examination of the problem

The considered "magnetohydrodynamic (MHD) two-fluid flow model pertains to a horizontal channel bounded by two parallel infinite plates extending in the *x*- and *z*-directions. The Cartesian coordinate system

is defined with the origin positioned midway between the plates (see Fig.1). The *x*-axis aligns with a hydrodynamic pressure gradient in the plane parallel to the channel plates but is not oriented toward the flow". It is presupposed that the width of the channel significantly exceeds its height.

Channel consists of two electrically conducting plates that are maintained at constant temperatures. These temperatures are denoted as T_{w1} at $y = h_1$ and T_{w2} at $y = h_2$. The upper region of the channel is referred to as region-I, while the lower region is designated as region-II. Region-I spans from $0 \leq y \leq h_1$, region-II covers the range $-h_2 \leq y \leq 0$. Investigating a two-dimensional magnetohydrodynamic (MHD) two-fluid flow, where ionized gases are propelled by a constant pressure gradient $\left(-\dfrac{\partial p}{\partial x} \right)$ through a horizontal channel between parallel plates, influenced by transverse electric and magnetic fields. The assumption is that the flow exhibits unsteady, laminar characteristics, and has reached full development.

The fluids within region I and region II are treated as immiscible, electrically conducting, incompressible substances with distinct densities (ρ_1 and ρ_2), viscosities (μ_1, μ_2) electrical conductivities $\left(\sigma_{01}, \sigma_{02} \right)$ and thermal conductivities (K_1, K_2). A constant-strength magnetic field $\left(B_0 \right)$ is applied in the *y*-direction, perpendicular to the channel, with consideration for the influence of Hall currents. The assumption of a small magnetic Reynolds number leads to the omission of the induced magnetic field.
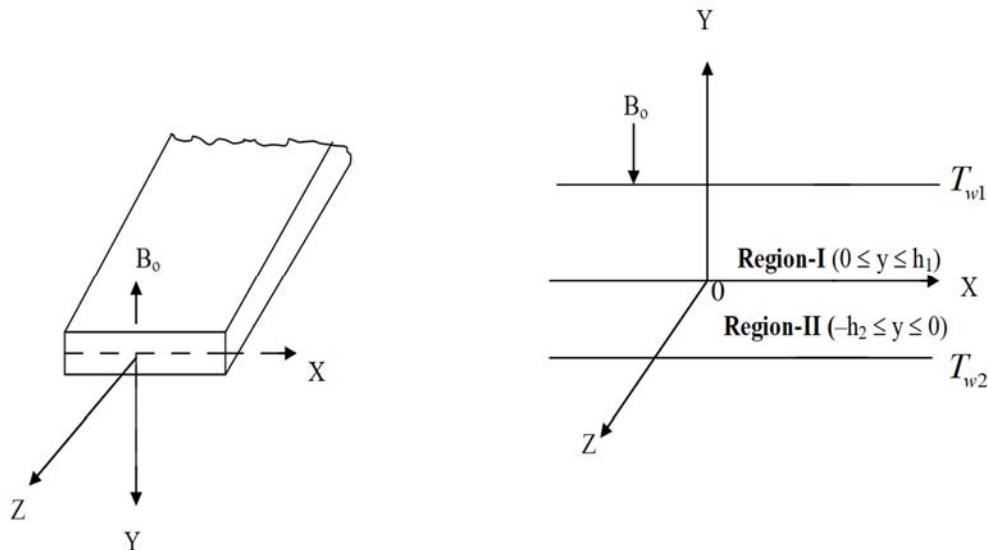

Fig.1. Flow scheme in coordinates.

The channel maintains strict boundaries to ensure stability, while the interface between the immiscible fluids is assumed to remain flat, stress-free, and undisturbed. Thermal boundary conditions are uniformly extended across the infinite channel plates, with thermal conduction in the flow direction and electron heating being disregarded. Given the infinite extension of the plates along the *x*- and *z*-directions, all physical variables, except pressure, are solely functions of *y* and *t*. With these considerations and insights from existing literature, governing equations for unsteady magnetohydrodynamic flow and heat transfer in a channel of parallel conducting plates, under transverse electric and magnetic fields within two-fluid regions, are formulated. This formulation is grounded in the fundamental equations for unsteady MHD flow of neutral fully ionized gas, accounting for Hall currents.

The governing equations in this investigation include the equations of motion, current, and energy, along with the corresponding boundary and interface conditions. The fundamental equations for an unsteady hydromagnetic flow of a neutral fully ionized gas in the presence of Hall currents as on the works of Spitzer[55] are given by:

Equation of motion:

$$\rho\left[\frac{\partial \overline{V}}{\partial t}+\left(\overline{V}.\nabla\right)\overline{V}\right]=-\nabla p+\mu\nabla^2\overline{V}+\left(\overline{J}\times\overline{B}\right).$$
(2.1)

Equation of current:

$$\overline{E}+\overline{V}\ x\ \overline{B}\ +\ \overline{E}_e-\frac{c}{en}\ \overline{J}\ x\ \overline{B}-\frac{\overline{J}}{\sigma_0}=0\ .$$
(2.2)

Equation of energy:

$$\rho\ c_p\left[\frac{\partial T}{\partial t}+\left(\overline{V}.\nabla\right)T\right]=K\ \nabla^2\ T+\phi+\left(\overline{J}^2\ /\ \sigma_0\right).$$
(2.3)

The continuity equation for an incompressible fluid:

$$\nabla.\overline{V}=0\ .$$
(2.4)

Given the aforementioned assumptions and employing the analytical approach akin to the works of Sato [5], L.Raju [46] and L.Raju and Valli [50], in the two fluid regions, we consider the fluid velocity $\overline{V}_i=(u_i,0,w_i),$ the magnetic flux intensity $\overline{B}=(0,B_0,0),$ the current density $\overline{J}_i=(J_{ix},0,J_{iz}),$ the electric field $\overline{E}_i=(E_{ix},0,E_{iz})$ and $J_i^2=J_{ix}^2+J_{iz}^2,(i=1,2)$ for both fluid regions. Consequently, the governing equations for the two-fluid regions, that is, the upper and lower regions denoted as Region-I and Region-II, are simplified and expressed as follows:

Region-I:

$$\rho_1\frac{\partial u_1}{\partial t}=\mu_1\frac{\partial^2 u_1}{\partial y^2}-\left\{1-s\left(1-\frac{\sigma_{11}}{\sigma_{01}}\right)\right\}\frac{\partial p}{\partial x}+\left\{-\sigma_{11}\left(E_{1z}+u_1 B_0\right)+\sigma_{21}\left(E_{1x}-w_1 B_0\right)\right\}B_0,$$
(2.5)

$$\rho_1\frac{\partial w_1}{\partial t}=\mu_1\frac{\partial^2 w_1}{\partial y^2}+s\frac{\partial p}{\partial x}\frac{\sigma_{21}}{\sigma_{01}}+\left\{\sigma_{11}\left(E_{1x}-w_1 B_0\right)+\sigma_{21}\left(E_{1z}+u_1 B_0\right)\right\}B_0,$$
(2.6)

$$\rho_1 c_{p_1}\frac{\partial T_1}{\partial t}\ -\ K_1\frac{\partial^2 T_1}{\partial y^2}=\mu_1\left\{\left(\frac{\partial u_1}{\partial y}\right)^2+\left(\frac{\partial w_1}{\partial y}\right)^2\right\}+\frac{J_1^2}{\sigma_{01}},$$
(2.7)

$$J_{1x}=\sigma_{11}E_{1x}-B_0\sigma_{11}w_1+\sigma_{21}E_{1z}+B_0\sigma_{21}u_1+\frac{\sigma_{21}}{\sigma_{01}}\frac{s}{B_0}\frac{\partial p}{\partial x},$$
(2.8)

$$J_{1z}=\left(\frac{E_{1z}}{B_0}+u_1\right)\sigma_{11}-\left(\frac{E_{1x}}{B_0}-w_1\right)\sigma_{21}+\left(\frac{\sigma_{11}}{\sigma_{01}}-1\right)\frac{s}{B_0}\frac{\partial p}{\partial x}\ .$$
(2.9)

Region-II:

$$\rho_2 \frac{\partial u_2}{\partial t} = \mu_2 \frac{\partial^2 u_2}{\partial y^2} - \left\{ 1 - s \frac{\partial p}{\partial x} \left(1 - \frac{\sigma_{12}}{\sigma_{02}} \right) \right\} + \left\{ -\sigma_{12} \left(E_{2z} + u_2 B_0 \right) + \sigma_{22} \left(E_{2x} - w_2 B_0 \right) \right\} B_0, \quad (2.10)$$

$$\rho_2 \frac{\partial w_2}{\partial t} = \mu_2 \frac{\partial^2 w_2}{\partial y^2} + \left(s \frac{\partial p}{\partial x} \frac{\sigma_{22}}{\sigma_{02}} \right) + \left\{ \sigma_{12} \left(E_{2x} - w_2 B_0 \right) + \sigma_{22} \left(E_{2z} + u_2 B_0 \right) \right\} B_0, \quad (2.11)$$

$$\rho_2 c_{p_2} \frac{\partial T_2}{\partial t} \; - \; K_2 \frac{\partial^2 T_2}{\partial y^2} = \mu_2 \left\{ \left(\frac{\partial u_2}{\partial y} \right)^2 + \left(\frac{\partial w_2}{\partial y} \right)^2 \right\} + \frac{J_2^2}{\sigma_{02}}, \quad (2.12)$$

$$J_{2x} = \sigma_{12} E_{2x} - B_0 \sigma_{12} w_2 + \sigma_{22} E_{2z} + B_0 \sigma_{22} u_2 + \frac{\sigma_{22}}{\sigma_{02}} \frac{s}{B_0} \frac{\partial p}{\partial x}, \quad (2.13)$$

$$J_{2z} = \left(\frac{E_{2z}}{B_0} + u_2 \right) \sigma_{12} - \left(\frac{E_{2x}}{B_0} - w_2 \right) \sigma_{22} + \left(\frac{\sigma_{12}}{\sigma_{02}} - 1 \right) \frac{s}{B_0} \frac{\partial p}{\partial x}. \quad (2.14)$$

The subscripts 1 and 2 in the above equations signify the quantities associated with regions I and II, respectively. The variables u_1, u_2 and w_1, w_2 represent the velocity components along the x- and z-directions in the two-fluid regions, referred to as primary and secondary velocity distributions. The notations E_{ix} and E_{iz}, J_{ix} and J_{iz} $(i = 1, 2)$ stand for the x- and z-components of the electric field and the current densities, respectively. The quantities T_1 and T_2 represent temperatures, and $c_{pi} (i = 1, 2)$ is the specific heat at constant pressure. The parameter s is defined as the ratio of electron pressure to the total pressure $(s = p_e / p)$, where values of $s = \frac{1}{2}$ and approximately zero correspond to neutral fully-ionized plasma and weakly-ionized gas, respectively. The coefficients σ_{11}, σ_{12} and σ_{21}, σ_{22} represent the modified conductivities parallel and normal to the direction of the electric field, respectively. Considering that T_{w1} and T_{w2} are constant everywhere on the upper and lower plates, respectively, the temperatures $\frac{\partial T_1}{\partial x} = 0, \frac{\partial T_1}{\partial z} = 0, \frac{\partial T_2}{\partial x} = 0, \frac{\partial T_2}{\partial z} = 0$ and T_1, T_2 are finite in the two-fluid regions and are functions of y and t only. The continuity of fluid velocity and shear stress is assumed over the interface at $y = 0$. The conditions on the temperature field enforce isothermal boundary conditions at the two plates, as well as the continuity of temperature and heat flux at the interface $y = 0$.

The boundary and interface conditions regarding velocity distributions are as follows:

$$u_1(h_1) \text{ and } w_1(h_1) = \begin{cases} 0 & \text{for } t \leq 0, \\ \text{Re} al \text{ of } \varepsilon e^{i\omega t} & \text{for } t > 0, \end{cases} \quad (2.15)$$

$$u_2(-h_2) = 0, \; w_2(-h_2) = 0, \quad (2.16)$$

$$u_1(0) = u_2(0), \; w_1(0) = w_2(0) \quad \text{for } h_1 = h_2, \quad (2.17)$$

$$\mu_1\left(\frac{\partial u_1}{\partial y}\right) = \mu_2\left(\frac{\partial u_2}{\partial y}\right) \quad \text{and} \quad \mu_1\left(\frac{\partial w_1}{\partial y}\right) = \mu_2\left(\frac{\partial w_2}{\partial y}\right) \quad \text{at } y = 0. \tag{2.18}$$

The isothermal boundary and interface conditions pertaining to temperature for both fluids are as follows:

$$T_1[h_1] = T_{w1}, \quad T_2[-h_2] = T_{w2}, \quad T_1[0] = T_2[0] \text{ for } h_1 = h_2,$$

$$K_1\left(\frac{\partial T_1}{\partial y}\right) = K_2\left(\frac{\partial T_2}{\partial y}\right) \text{ at } y = 0, \tag{2.19}$$

The ensuing non dimensional variables are employed in formulating the governing equations (2.5) through (2.14) and (2.15) to (2.19) in a dimensionless manner:

$$u^\bullet_1 = \frac{u_1}{u_p}, \quad u^\bullet_2 = \frac{u_2}{u_p}, \quad w^\bullet_1 = \frac{w_1}{u_p}, \quad w^\bullet_2 = \frac{w_2}{u_p}, \quad y^\bullet_i = \frac{y_i}{h_i}, \quad u_p = -\frac{\partial p}{\partial x}\frac{h_1^2}{\mu_1},$$

$$t^\bullet = \frac{\mu_i t}{\rho_i h_i^2}, \quad \omega^\bullet = \frac{\omega h_i^2 \rho_i}{\mu_i}, \quad (i = 1, 2), \quad m_{ix} = \frac{E_{ix}}{B_0 u_p}, \quad m_{iz} = \frac{E_{iz}}{B_0 u_p},$$

$$I_{ix} = \frac{J_{ix}}{\sigma_{0i} B_0 u_p}, \quad I_{iz} = \frac{J_{iz}}{\sigma_{0i} B_0 u_p}, \quad J_i^2 = J_{ix}^2 + J_{iz}^2,$$

$$M \text{ (Hartmann number)} = B^2_0 h^2_1\left(\frac{\sigma_{01}}{\mu_1}\right), \quad \alpha \text{ (the viscosity ratios)} = \frac{\mu_1}{\mu_2},$$

$$h \text{ (the height ratios)} = \frac{h_2}{h_1}, \rho \text{ (the density ratios)} = \frac{\rho_2}{\rho_1}, \tag{2.20}$$

$$\sigma_0 \text{ (ratio of the electrical conductivities)} = \frac{\sigma_{01}}{\sigma_{02}},$$

$$\sigma_{01} = \frac{\sigma_{12}}{\sigma_{11}}, \quad \sigma_{02} = \frac{\sigma_{22}}{\sigma_{21}}, \quad \frac{\sigma_{11}}{\sigma_{01}} = \frac{1}{1 + m^2}, \quad \frac{\sigma_{21}}{\sigma_{01}} = \frac{m}{1 + m^2},$$

$$m \text{ (Hall parameter)} = \frac{\omega_e}{\left(\frac{1}{\tau} + \frac{1}{\tau_e}\right)},$$

$$\beta \text{ (the proportion of thermal conductivities between the two fluids)} = \frac{K_1}{K_2},$$

$$\theta_i \text{ (distribution of temperature)} = \frac{T_i - T_{wi}}{\left(u_p^2 \mu_1 / K_i\right)}.$$

In this context, ω_e represents the gyration frequency of electrons, while τ and τ_e denote the mean collision time between electrons and ions, and electrons and neutral particles, respectively. The provided expression for the Hall parameter m, applicable to partially-ionized gases, coincides with that of fully-ionized gases as τ_e approaches infinity.

Utilizing the transformations outlined above (in Eq.2.20) and disregarding the asterisks, Eqs (2.5) to (2.14) assume their non-dimensional form. Moreover, the channel side plates are thought to be short-circuited by an outside conductor and comprised of conducting material, causing the induced electric current to flow out of the channel. Hence, there is no electric potential between the channel plates. We also have $m_x = 0, m_z = 0$ if we accept no electric field in the *x* and *z* axes (see Sato [5], L.Raju [46] and L.Raju and Venkat [51]). As a result, the dimensionless governing equations of motion, current, energy, and conditions in the two zones take the following form.

Region-I

$$\frac{\partial u_1}{\partial t} + \lambda \frac{\partial u_1}{\partial y} = \frac{\partial^2 u_1}{\partial y^2} - \frac{M^2 u_1}{1+m^2} - \frac{M^2 m w_1}{1+m^2} + \beta_1, \tag{2.21}$$

$$\frac{\partial w_1}{\partial t} + \lambda \frac{\partial w_1}{\partial y} = \frac{\partial^2 w_1}{\partial y^2} - \frac{M^2 w_1}{1+m^2} + \frac{M^2 m u_1}{1+m^2} + \beta_2, \tag{2.22}$$

$$\frac{d\theta_1}{dt} - \lambda \frac{\partial \theta_1}{\partial y} = \frac{1}{P_{r1}} \frac{\partial^2 \theta_1}{\partial y^2} + \left\{ \left(\frac{\partial u_1}{\partial y} \right)^2 + \left(\frac{\partial w_1}{\partial y} \right)^2 \right\} + M^2 I_1^2, \tag{2.23}$$

$$I_{1x} = \frac{m u_1}{1+m^2} - \frac{w_1}{1+m^2} - \frac{s}{M^2} \frac{m}{1+m^2}, \tag{2.24}$$

$$I_{1z} = \frac{u_1}{1+m^2} + \frac{m w_1}{1+m^2} + \frac{s}{M^2} \left(1 - \frac{m}{1+m^2} \right) \tag{2.25}$$

and $I_1^2 = I_{1x}^2 + I_{1z}^2$.

Region-II

$$\frac{\partial u_2}{\partial t} + \rho \alpha h \lambda \frac{\partial u_2}{\partial y} = \frac{\partial^2 u_2}{\partial y^2} - \frac{\alpha \sigma_1 h^2 M^2 u_2}{1+m^2} - \frac{m \alpha \sigma_2 h^2 M^2 w_2}{1+m^2} + \beta_3 \alpha h^2, \tag{2.26}$$

$$\frac{\partial w_2}{\partial t} + \rho \alpha h \lambda \frac{\partial w_2}{\partial y} = \frac{\partial^2 w_2}{\partial y^2} - \frac{\alpha \sigma_1 h^2 M^2 w_2}{1+m^2} + \frac{m \alpha \sigma_2 h^2 M^2 u_2}{1+m^2} + \beta_4 \alpha h^2, \tag{2.27}$$

$$\frac{d\theta_2}{dt} - h \rho \alpha \lambda \frac{d\theta_2}{dy} = \frac{1}{P_{r2}} \frac{d^2 \theta_2}{dy^2} + \frac{\beta}{\alpha} \left\{ \left(\frac{du_2}{dy} \right)^2 + \left(\frac{dw_2}{dy} \right)^2 \right\} + h^2 \sigma \beta M^2 I_2^2, \tag{2.28}$$

$$I_{2x} = \frac{m\sigma_0\sigma_2 u_2}{1+m^2} - \frac{\sigma_0\sigma_1 w_2}{1+m^2} - \frac{s\sigma_0{}^2\sigma_2}{M^2}\frac{m}{1+m^2}\,, \tag{2.29}$$

$$I_{2z} = \frac{\sigma_0\sigma_1 u_2}{1+m^2} + \frac{m\sigma_0\sigma_2 w_2}{1+m^2} + \left(1 - \frac{\sigma_0\sigma_1}{1+m^2}\right)\frac{s\sigma_0}{M^2}\,, \tag{2.30}$$

and $\quad I_2{}^2 = I_{2x}{}^2 + I_{2z}{}^2$

where

$$\beta_1 = 1 - s\left(\frac{1}{1+m^2}\right), \quad \beta_2 = \frac{-sm}{1+m^2}, \quad \beta_3 = 1 - s\left(1 - \frac{\sigma_0\sigma_{01}}{1+m^2}\right), \quad \beta_4 = \frac{-s\sigma_0\sigma_{02}m}{1+m^2}.$$

The boundary and interface conditions on u_1, w_1 and u_2, w_2 are given by:

$$u_1(1) = \begin{cases} 0 & \text{for } t \le 0, \\ \varepsilon\cos\omega t & \text{for } t > 0, \end{cases} \quad \text{and} \quad w_1(1) = \begin{cases} 0 & \text{for } t \le 0, \\ \varepsilon\cos\omega t & \text{for } t > 0, \end{cases} \tag{2.31}$$

$$u_2(-1) = 0, \quad w_2(-1) = 0\,, \tag{2.32}$$

$$u_1(0) = u_2(0),\, w_1(0) = w_2(0)\,, \tag{2.33}$$

$$\frac{\partial u_1}{\partial y} = \left(\frac{1}{\alpha h}\right)\frac{\partial u_2}{\partial y}, \quad \frac{\partial w_1}{\partial y} = \left(\frac{1}{\alpha h}\right)\frac{\partial w_2}{\partial y} \quad \text{and} \quad \mu_1\frac{\partial w_1}{\partial y} = \mu_2\frac{\partial w_2}{\partial y} \quad \text{at } y = 0. \tag{2.34}$$

The boundary and interface conditions on temperature for both fluids are:

$$\theta_1(1) = 0, \quad \theta_2(-1) = 0, \quad \theta_1(0) = \theta_2(0) \quad \text{and} \quad \frac{\partial\theta_1}{\partial y} = \frac{1}{\beta h}\frac{\partial\theta_2}{\partial y} \quad \text{at } y = 0\,. \tag{2.35}$$

3. Solution methodology

Our objective is to address the equations governing momentum and energy (2.21, 2.22, 2.23, 2.26, 2.27 and 2.28), taking into account the boundary and interface conditions (2.31 to 2.35), in order to determine the velocity and temperature distributions within the fluid domains. These equations form a complex system of interconnected partial differential equations, devoid of direct solutions. Nonetheless, we can streamline them into ordinary linear differential equations utilizing the first-order regular perturbation method, under the assumption of a two-term series expansion:

$$u_1(y,t) = u_{01}(y) + \text{Re}\,al\, of\, \varepsilon e^{i\omega t} u_{11}(y),$$

$$\text{for} \quad t > 0\,, \tag{3.1}$$

$$w_1(y,t) = w_{01}(y) + \text{Re}\,al\, of\, \varepsilon e^{i\omega t} w_{11}(y),$$

$$u_2(y,t) = u_{02}(y) + \mathrm{Re}\,al\;of\;\varepsilon e^{i\omega t}\,u_{12}(y),$$

$$\text{for}\quad t > 0, \tag{3.2}$$

$$w_2(y,t) = w_{02}(y) + \mathrm{Re}\,al\;of\;\varepsilon e^{i\omega t}\,w_{12}(y),$$

$$\theta_1(y,t) = \theta_{01}(y) + \mathrm{Re}\,al\;of\;\varepsilon e^{i\omega t}\,\theta_{11}(y),$$

$$\text{for}\quad t > 0. \tag{3.3}$$

$$\theta_2(y,t) = \theta_{02}(y) + \mathrm{Re}\,al\;of\;\varepsilon e^{i\omega t}\,\theta_{12}(y),$$

In this context, the variables $u_{01}(y)$, $u_{02}(y)$, $w_{01}(y)$, $w_{02}(y)$ and $\theta_{01}(y)$, $\theta_{02}(y)$ signify the stable elements of velocity and temperature distributions within the two distinct fluid domains. Conversely, the variables $u_{11}(y)$, $u_{12}(y)$, $w_{11}(y)$, $w_{12}(y)$ and $\theta_{11}(y)$, $\theta_{12}(y)$ represent the dynamic components that evolve with time, pivotal in resolving the posed issue.

In order to set the Eqs (2.21) and (2.22) into a single equation and for simplicity, we introduce a complex function $q_1(y,t) = u_1(y,t) + iw_1(y,t)$; likewise $q_2(y,t) = u_2(y,t) + iw_2(y,t)$ to combine the Eqs (2.26) and (2.27). Thereby utilizing the expressions given in the Eqs (3.1-3.3) into the Eqs (2.21-2.23 and 2.26-2.28) and then separating the steady and transient time-varying parts, we obtain the following differential equations in terms of the complex notations, namely q_{01}, q_{11}, q_{02} and q_{12}; where $q_{01} = u_{01} + iw_{01}$, $q_{11} = u_{11} + iw_{11}$, $q_{02} = u_{02} + iw_{02}$, $q_{12} = u_{12} + iw_{12}$.

Region-I
For steady-state part

$$\frac{d^2 q_{01}}{dy^2} - a_1 q_{01} = a_2, \tag{3.4}$$

$$\frac{1}{P_r}\frac{d^2\theta_{01}}{dy^2} = -b_1 e^{(m_1 + \overline{m_1})y} - b_2 e^{(m_1 + \overline{m_2})y} - b_3 e^{(m_2 + \overline{m_1})y} +$$
$$-b_4 e^{(m_2 + \overline{m_2})y} - b_5 e^{m_1 y} - b_6 e^{m_2 y} - b_7 e^{\overline{m_1} y} - b_8 e^{\overline{m_2} y} - b_9. \tag{3.5}$$

For transient time dependent part

$$\frac{d^2 q_{11}}{dy^2} - (a_1 - \omega\tan\omega t)q_{11} = 0, \tag{3.6}$$

$$\frac{1}{P_r}\frac{d^2\theta_{11}}{dy^2} + (\omega\tan\omega t)\theta_{11} = b_{66} e^{(m_5 + \overline{m_5})y} + b_{67} e^{(m_5 + \overline{m_6})y} + b_{68} e^{(m_6 + \overline{m_5})y} +$$
$$+b_{69} e^{(m_6 + \overline{m_6})y} + b_{62} e^{\overline{m_5} y} + b_{63} e^{\overline{m_6} y} + b_{64} e^{m_5 y} + b_{65} e^{m_6 y}. \tag{3.7}$$

Region-II
For steady-state part

$$\frac{d^2 q_{02}}{dy^2} - a_3 q_{02} = a_4, \tag{3.8}$$

$$\frac{1}{P_r}\frac{d^2\theta_{02}}{dy^2} = -b_{28}e^{(m_3+\overline{m_3})y} - b_{29}e^{(m_3+\overline{m_4})y} - b_{30}e^{(m_4+\overline{m_3})y} +$$

$$-b_{31}e^{(m_4+\overline{m_4})y} - b_{32}e^{m_3 y} - b_{33}e^{m_4 y} - b_{34}e^{\overline{m_3}y} - b_{35}e^{\overline{m_4}y} - b_{27}. \tag{3.9}$$

For transient time dependent part

$$\frac{d^2q_{12}}{dy^2} - (a_3 - \omega\tan\omega t)q_{12} = 0, \tag{3.10}$$

$$\frac{1}{P_r}\frac{d^2\theta_{12}}{dy^2} + (\omega\tan\omega t)\theta_{12} = b_{90}e^{(m_7+\overline{m_7})y} + b_{91}e^{(m_7+\overline{m_8})y} + b_{92}e^{(m_8+\overline{m_7})y} +$$

$$+b_{93}e^{(m_8+\overline{m_8})y} + b_{86}e^{\overline{m_7}y} + b_{87}e^{\overline{m_8}y} + b_{88}e^{m_7 y} + b_{89}e^{m_8 y}. \tag{3.11}$$

Exploring the scenario of conductive plates

If the lateral plates are constructed from conductive materials and experience a short circuit through an external conductor, the resulting induced electric current exits the conduit. In this scenario, no electric potential is present between the side plates. Furthermore, assuming zero electric field in the *x*- and *z*-directions, we establish $m_x = 0$, $m_z = 0$ (see Sato [5]). The constants in the arrangement are determined based on these two conditions. The solutions for u_1, u_2; w_1, w_2; u_{m_1}, u_{m_2}; w_{m_1}, w_{m_2}, I_1 and I_2 in the two regions are derived as follows:

Region-I
In the steady-state case

$$q_{01}(y) = u_{01}(y) + iw_{01}(y) = A_1e^{m_1 y} + A_2e^{m_2 y} - \frac{a_2}{a_1}. \tag{3.12}$$

In the time-dependent transient component

$$q_{11}(y) = u_{11}(y) + iw_{11}(y) = A_5e^{m_5 y} + A_6e^{m_6 y}, \tag{3.13}$$

$$I_1 = I_{1x} + iI_{1z} = \left(\frac{1}{1+m^2}\right)(iu_1 - w_1) + \left(\frac{m}{1+m^2}\right)(u_1 + iw_1) +$$

$$-\frac{s}{M^2}\left(\frac{m}{1+m^2} - i\left(1 - \frac{m}{1+m^2}\right)\right), \tag{3.14}$$

$$q_1(y,t) = q_{01}(y) + \varepsilon\cos\omega t . q_{11}(y) = A_1e^{m_1 y} + A_2e^{m_2 y} - \frac{a_2}{a_1} + \varepsilon\cos\omega t\left(A_5e^{m_5 y} + A_6e^{m_6 y}\right). \tag{3.15}$$

The complex form of the mean velocity is given by:

$$q_{m_1} = u_{m_1} + iw_{m_1} = \int_0^1 q_1 dy = A_1a_{97} + A_2a_{98} - \frac{a_2}{a_1} + A_{28}. \tag{3.16}$$

Region-II
In the steady-state case

$$q_{02}(y) = u_{02}(y) + iw_{02}(y) = A_3 e^{m_3 y} + A_4 e^{m_4 y} - \frac{a_4}{a_3}. \tag{3.17}$$

In the time-dependent transient component

$$q_{12}(y) = u_{12}(y) + iw_{12}(y) = A_7 e^{m_7 y} + A_8 e^{m_8 y}, \tag{3.18}$$

$$I_2 = I_{2x} + iI_{2z} = \left(\frac{\sigma_0 \sigma_{01}}{1+m^2}\right)(iu_2 - w_2) + \left(\frac{m\sigma_0 \sigma_{02}}{1+m^2}\right)(u_2 + iw_2) +$$
$$-\frac{s\sigma_0^2 \sigma_{02}}{M^2}\left(\frac{m}{1+m^2}\right) + \frac{s\sigma_0 i}{M^2} - \frac{s\sigma_0^2 \sigma_{01} i}{\left(1+m^2\right)M^2}, \tag{3.19}$$

$$q_2(y,t) = q_{02}(y) + \varepsilon\cos\omega t . q_{12}(y) = A_3 e^{m_3 y} + A_4 e^{m_4 y} - \frac{a_4}{a_3} + \varepsilon\cos\omega t\left(A_7 e^{m_7 y} + A_8 e^{m_8 y}\right). \tag{3.20}$$

The mean velocity is given by:

$$q_{m_2} = u_{m_2} + iw_{m_2} = \int_0^1 q_2 dy = A_3 a_{99} + A_4 a_{100} - \frac{a_4}{a_3} + A_{29}. \tag{3.21}$$

In the scenario of conducting plates temperature:

The energy equations in simplified form of this case are given by,

Region-I

$$\frac{\partial\theta_1}{\partial t} - \frac{1}{p_r}\frac{\partial^2\theta_1}{\partial y^2} = \left(\frac{\partial U_1}{\partial y}\right)\left(\frac{\partial \overline{U_1}}{\partial y}\right) + M^2\left\{\frac{1}{1+m^2}\left(U_1\overline{U_1}\right) + \right.$$
$$\left. + \left(1 - \frac{1}{1+m^2}\right)\frac{s^2}{M^4}\frac{1}{q_{m_1}\overline{q_{m_1}}} + \frac{is}{M^2}\frac{m}{1+m^2}\left(\frac{\overline{U_1}}{q_{m_1}} - \frac{U_1}{\overline{q_{m_1}}}\right)\right\}, \tag{3.22}$$

$$\theta_1(y,t) = \left(b_{251}e^{b_{23}y} + b_{252}e^{b_{24}y} + b_{253}e^{b_{25}y} + b_{47}e^{b_{26}y} + b_{254}e^{m_1 y} + b_{255}e^{m_2 y} + b_{256}e^{\overline{m_1}y} + \right.$$
$$+ b_{257}e^{\overline{m_2}y} + b_{258}y^2\right) + B_9 y + B_{10} + \varepsilon\cos\omega t\left(B_{13}e^{b_{120}y} + B_{14}e^{-b_{120}y} + b_{146}e^{b_{138}y} + \right. \tag{3.23}$$
$$\left. + b_{147}e^{b_{139}y} + b_{148}e^{b_{140}y} + b_{149}e^{b_{141}y} + b_{297}e^{\overline{m_5}y} + b_{298}e^{\overline{m_6}y} + b_{299}e^{m_5 y} + b_{300}e^{m_6 y}\right),$$

The heat transfer coefficient rate at the upper plate $Nu_1 = -\left(\dfrac{d\theta_1}{dy}\right)$ at $y = 1$,

$$Nu_1 = -\Big[\big(b_{251}b_{23}e^{b23} + b_{252}b_{24}e^{b24} + b_{253}b_{25}e^{b25} + b_{47}b_{26}e^{b26} + b_{254}m_1e^{m1} +$$

$$b_{255}m_2e^{m2} + b_{256}\overline{m_1}e^{\overline{m_1}} + b_{257}\overline{m_2}e^{\overline{m_2}}\big) + 2b_{258} + B_9 + \varepsilon\cos\omega t\big(B_{13}b_{120}e^{b120} -$$

$$+ B_{14}b_{120}e^{-b120} + b_{146}b_{138}e^{b138} + b_{147}b_{139}e^{b139} + b_{148}b_{140}e^{b140} + b_{149}b_{141}e^{b141} +$$

$$+ b_{297}\overline{m_5}e^{\overline{m_5}} + + b_{298}\overline{m_6}e^{\overline{m_6}} + b_{299}m_5e^{m5} + b_{300}m_6e^{m6}\big)\Big]. \tag{3.24}$$

Region-II

$$\frac{\partial\theta_2}{\partial t} - \frac{1}{p_r}\frac{\partial^2\theta_2}{\partial y^2} = \frac{\beta}{\alpha}\left(\frac{\partial U_2}{\partial y}\right)\left(\frac{\partial\overline{U_2}}{\partial y}\right) + M^2h^2\beta\left\{\frac{\sigma_1}{1+m^2}\left(U_2\overline{U_2}\right) + \right.$$

$$\left. + \left(1 - \frac{\sigma_1}{1+m^2}\right)\frac{s^2}{M^4}\frac{1}{q_{m_2}\overline{q_{m_2}}} + \frac{is}{M^2}\frac{\sigma_2 m}{1+m^2}\left(\frac{\overline{U_2}}{q_{m_2}} - \frac{U_2}{\overline{q_{m_2}}}\right)\right\}, \tag{3.25}$$

$$\theta_2(y,t) = b_{94}e^{b74y} + b_{95}e^{b75y} + b_{96}e^{b76y} + b_{97}e^{b77y} + b_{274}e^{m3y} + b_{275}e^{m4y} + b_{276}e^{\overline{m3}y} +$$

$$+ b_{277}e^{\overline{m4}y} + b_{278}y^2 + B_{11}y + B_{12} + \varepsilon\cos\omega t\big(B_{15}e^{b120y} + B_{16}e^{-b120y} + b_{317}e^{b185y} +$$

$$+ b_{318}e^{b186y} + b_{195}e^{b187y} + b_{196}e^{b188y} + b_{319}e^{m7y} + b_{320}e^{m8y} + b_{321}e^{\overline{m7}y} + b_{322}e^{\overline{m8}y}\big), \tag{3.26}$$

The heat transfer coefficient rate at the lower plate $Nu_2 = \frac{1}{\beta h}\left(\frac{d\theta_2}{dy}\right)$ at $y = -1$,

$$Nu_2 = \frac{1}{\beta h}\Big[\big(b_{94}b_{74}e^{-b74} + b_{95}b_{75}e^{-b75} + b_{96}b_{76}e^{-b76} + b_{97}b_{77}e^{-b77} + b_{274}m_3e^{-m3} +$$

$$+ b_{275}m_4e^{-m4} + b_{276}\overline{m_3}e^{-\overline{m3}} + b_{277}\overline{m_4}e^{-\overline{m4}}\big) - 2b_{278} + B_{11} + \varepsilon\cos\omega t\big(B_{15}b_{120}e^{-b120} -$$

$$+ B_{16}b_{120}e^{b120} + b_{317}b_{185}e^{-b185} + b_{318}b_{186}e^{-b186} + b_{195}b_{187}e^{-b187} + b_{196}b_{188}e^{-b188} +$$

$$+ b_{319}m_7e^{-m7} + b_{320}m_8e^{-m8} + b_{321}\overline{m_7}e^{-\overline{m7}} + b_{322}\overline{m_8}e^{-\overline{m8}}\big)\Big]. \tag{3.27}$$

4. Results and discussion

The equations governing the unsteady scenario of conducting plates involve primary formulations for motion, current, and energy. Utilizing these equations, the main and transverse velocity fields, referred to as u_1, u_2 and w_1, w_2, as well as the temperature fields θ_1, θ_2 and in the two fluids. The solution to these equations is obtained and visualized in Figs 1 to 43. Unsteady flow patterns are represented by solid lines, while dash-spot lines depict steady flow motions. The impact of control parameters, including the Hartmann number M, Hall parameter m, viscosity ratio α, height ratio h, as well as ratio of electrical conductivity σ_0, density ratio ρ and β (ratios of electrical and heat conductivities), on the flow and temperature fields is explored for two scenarios: $(s=0)$ and s equal to half of its estimate. In the numerical calculations, values such as ($\sigma_{01} = 1.2$, $\sigma_{02} = 1.5$, $P_{r_1} = P_{r_2} = 1$) are utilized. Notably, in contrast to scenarios with conducting plates, the solutions in

the present study are observed to depend on s (electron pressure to total pressure ratio) when the plates exhibit conducting properties. The theoretical outcomes of this study align with those presented by L.Raju [46] for a steady flow with non-porous plates and without the rotation component. Also, the results of this study coincides with those of L.Raju and Venkat [51] in absence of rotation and when the plates are non-porous in nature.

When considering the scenario where the electron-to-total pressure ratio s is equal to zero:

The impact of varying the Hartmann number M on the velocity distribution in both regions is depicted in Figs 2 and 3. In Fig.2, an increase in M is associated with a decrease in the primary velocity distribution in both regions. Fig.3 demonstrates that increasing the Hartmann number M up to ($M < 4$) enhances the secondary velocity distribution, while for ($M>4$) the secondary velocity distribution diminishes in both regions. Additionally, it is observed that the maximum velocity in the channel tends to shift towards region-I over the channel centreline. Analyzing the effect of varying the Hartmann number M on the temperature distribution, Fig.4 shows that an increase in M leads to a reduction in the temperature distribution in both regions. As M increases, the maximum temperature in the channel tends to move below the channel centreline towards region-II, while all other governing parameters remain constant.
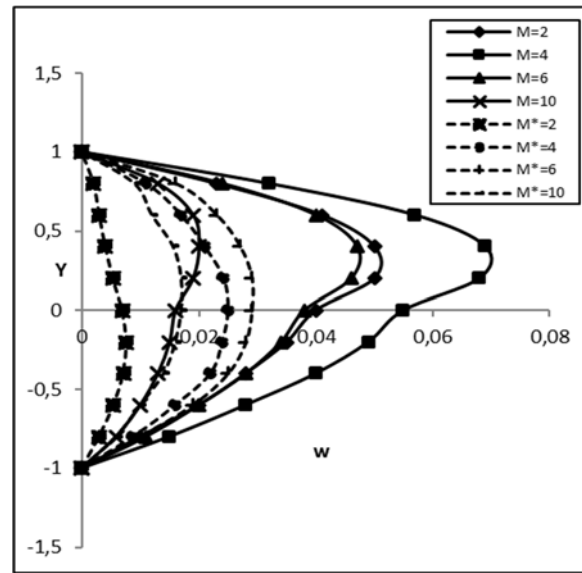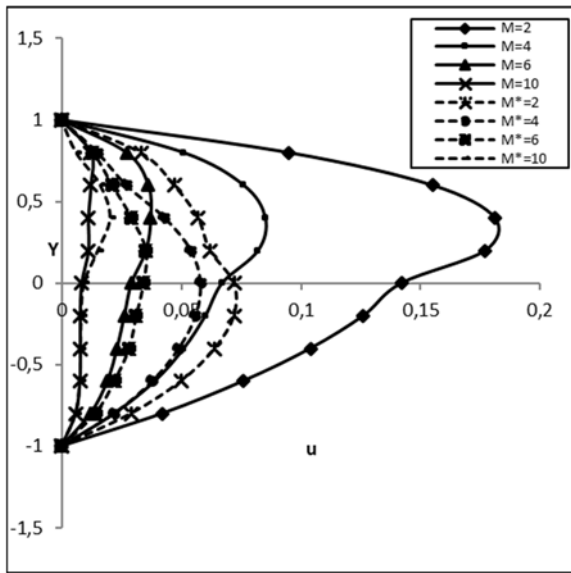
Fig.2. Depicts velocity profiles (primary) for unsteady flow (u_1, u_2) and the steady case (u_1^*, u_2^*) across varying M, with specific parameters: $h = 0.75$, $m = 2$, $\alpha = 0.333$, $\sigma_0 = 2$, $\sigma_{01} = 1.2$, $s = 0$, $\sigma_{02} = 1.5$, $\varepsilon = 0.5$, $\rho = 1$, $t = \pi / \omega$, $\omega = 1$.

Fig.3. Depicts velocity profiles (secondary) for unsteady flow (w_1, w_2) and the steady case (w_1^*, w_2^*) across varying M, with specific parameters: $h = 0.75$, $m = 2$, $\alpha = 0.333$, $\sigma_0 = 2$, $\sigma_{01} = 1.2$, $s = 0$, $\sigma_{02} = 1.5$, $\varepsilon = 0.5$, $\rho = 1$, $t = \pi / \omega$, $\omega = 1$.

Figures 5 and 6 depict the impact of varying the Hall parameter 'm' on velocity distributions in two distinct regions. In Fig.5, it is evident that an increase in m enhances the primary velocity distribution across both regions. Meanwhile, Fig.6 illustrates that an increase in the Hall parameter (m) up to the value of $(m = 2)$ amplifies the secondary velocity distribution; however, beyond this threshold, the secondary velocity distribution diminishes in both regions. As m increase the maximum primary and secondary velocity distributions in the channel tend to shift over the channel centerline towards region-I.
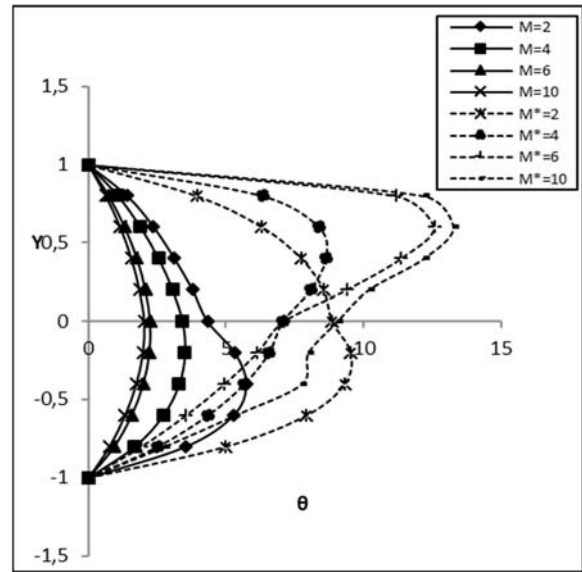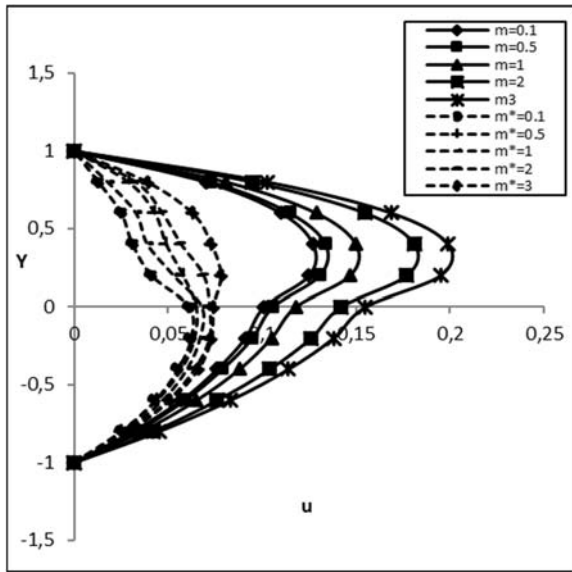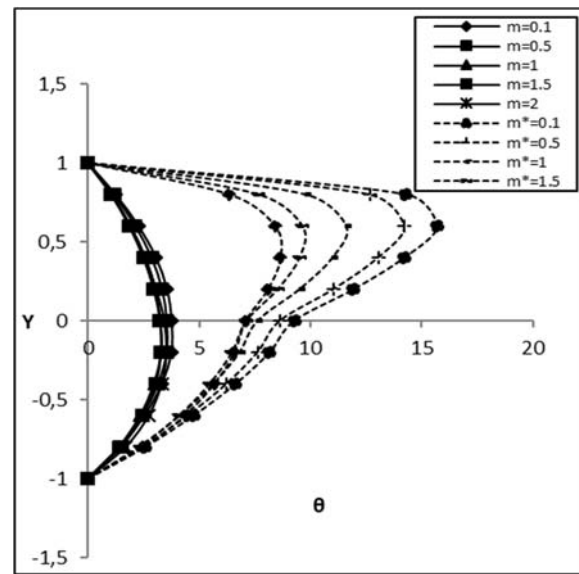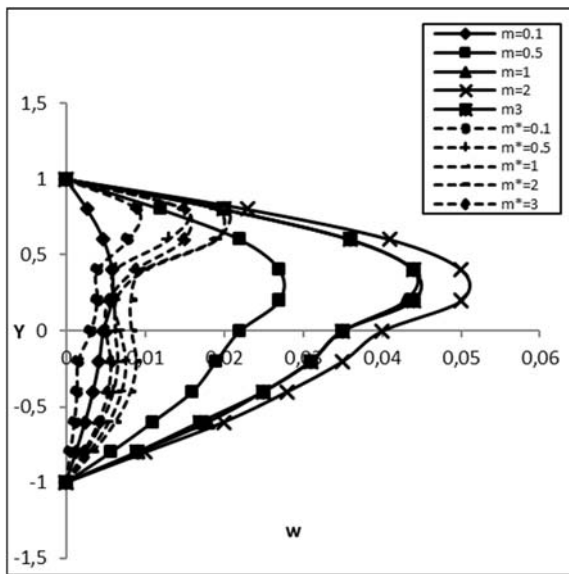
Fig.4. Depicts temperature profiles for unsteady flow $\left(\theta_1, \theta_2\right)$ and the steady case $\left(\theta_1^*, \theta_2^*\right)$ across varying M, with specific parameters:
$h = 0.75, m = 2, \alpha = 0.333, \sigma_0 = 2, \sigma_{01} = 1.2, s = 0,$
$\sigma_{02} = 1.5, \varepsilon = 0.5, \rho = 1, t = \pi / \omega, \beta = 0.5, \omega = 1.$

Fig.5. Depicts velocity profiles (primary) for unsteady flow $\left(u_1, u_2\right)$ and the steady case $\left(u_1^*, u_2^*\right)$ across varying m, with specific parameters:
$h = 0.75, M = 2, \alpha = 0.333, \sigma_0 = 2, \sigma_{01} = 1.2,$
$\sigma_{02} = 1.5, \varepsilon = 0.5, \rho = 1, t = \pi / \omega, \omega = 1, s = 0.$

Fig.6. Depicts velocity profiles (secondary) for unsteady flow $\left(w_1, w_2\right)$ and the steady case $\left(w_1^*, w_2^*\right)$ across varying m, with specific parameters:
$h = 0.75, M = 2, \alpha = 0.333, \sigma_0 = 2, \sigma_{01} = 1.2, s = 0,$
$\sigma_{02} = 1.5, \varepsilon = 0.5, \rho = 1, t = \pi / \omega, \omega = 1.$

Fig.7. Depicts temperature profiles for unsteady flow $\left(\theta_1, \theta_2\right)$ and the steady case $\left(\theta_1^*, \theta_2^*\right)$ across varying m, with specific parameters:
$h = 0.75, M = 4, \alpha = 0.333, \sigma_0 = 2, \sigma_{01} = 1.2, s = 0,$
$\sigma_{02} = 1.5, \varepsilon = 0.5, \rho = 1, t = \pi / \omega, \beta = 0.5, \omega = 1.$

The influence of the Hall parameter m on temperature distribution is examined in Fig.7. The results reveal that in region-I, an increase in the Hall parameter m leads to a reduction in the temperature distribution.

Conversely, in region-II, the temperature distribution decreases up to $(m = 1)$ and then starts increasing. Additionally, as the Hall parameter m increases, the maximum temperature in the channel tends to shift over the channel centreline towards region-I.
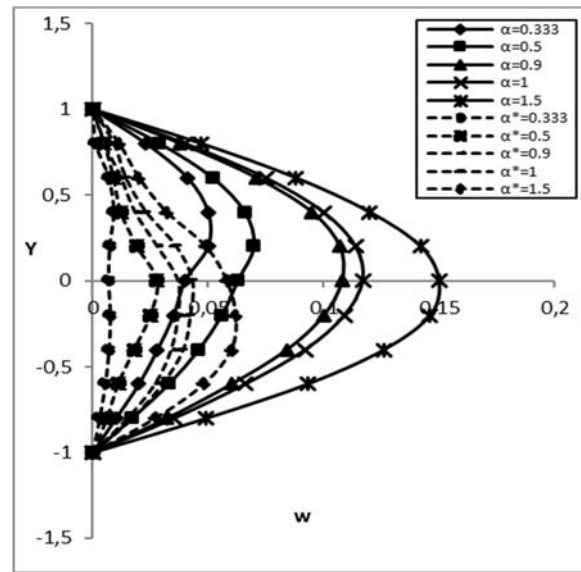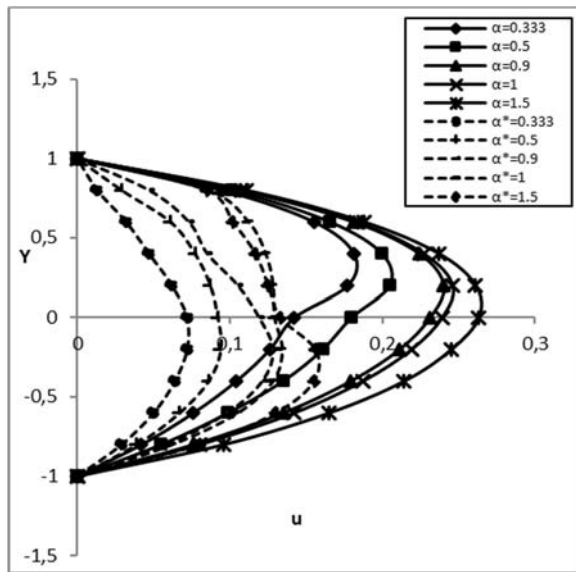

Fig.8. Depicts velocity profiles (primary) for unsteady flow (u_1, u_2) and the steady case (u_1^*, u_2^*) across varying α, with specific parameters: $h = 0.75$, $M = 2$, $m = 2$, $\sigma_0 = 2$, $\sigma_{01} = 1.2$, $s = 0$, $\sigma_{02} = 1.5$, $\varepsilon = 0.5$, $\rho = 1$, $t = \pi / \omega$, $\omega = 1$.

Fig.9. Depicts velocity profiles (secondary) for unsteady flow (w_1, w_2) and the steady case (w_1^*, w_2^*) across varying α, with specific parameters: $h = 0.75$, $M = 2$, $m = 2$, $\sigma_0 = 2$, $\sigma_{01} = 1.2$, $\sigma_{02} = 1.5$, $\varepsilon = 0.5$, $\rho = 1$, $t = \pi / \omega$, $\omega = 1$, $s = 0$.

The impact of the viscosity ratio α is depicted in Figs 8 and 9. In Fig.8, it is evident that an increase in α enhances the primary velocity distribution in both regions, with the exception of the upper side plate where the profile shows no significant variation. Fig.9 demonstrates that an increase in α amplifies the secondary velocity distributions in both regions. As α increases, the maximum primary and secondary velocity distributions in the channel tend to shift over the channel centreline towards region-I. An examination of the influence of the viscosity ratio on temperature distribution is presented in Fig.10. It shows that an increase in α enhances the temperature distribution up to a certain value, beyond which it decreases in both regions. Additionally, the temperature distribution in the channel tends to shift below the channel centreline towards region-II as α increments.

The impact of the height ratio h on primary and secondary velocity distributions is illustrated in Figs 11 and 12. Figure 11 shows that an increase in h enhances the primary velocity distribution in both regions, with no significant variation observed near the side plates. In Fig.12, an expansion in h is observed to amplify the secondary velocity distributions in both regions. As h increases, the maximum primary and secondary velocity distributions in the channel tend to shift over the channel centreline towards region-I. Analyzing the effect of varying the height ratio 'h' on temperature distribution, Fig.13 indicates that an increase in the height ratio enhances the temperature distribution in both regions. Moreover, the maximum temperature in the channel tends to shift below the channel centreline towards region-II as h increases.
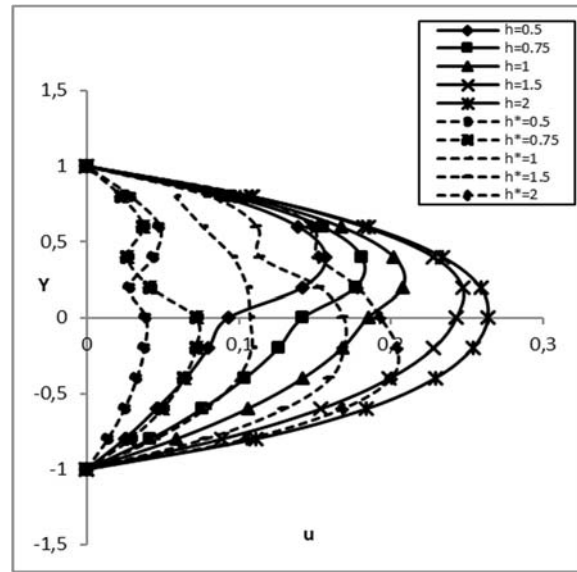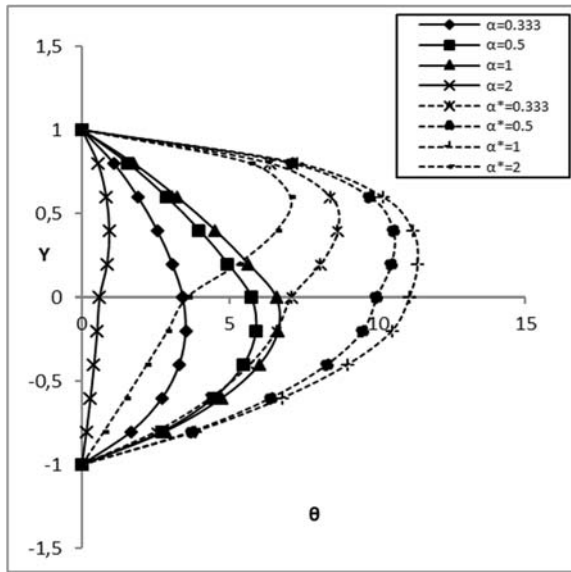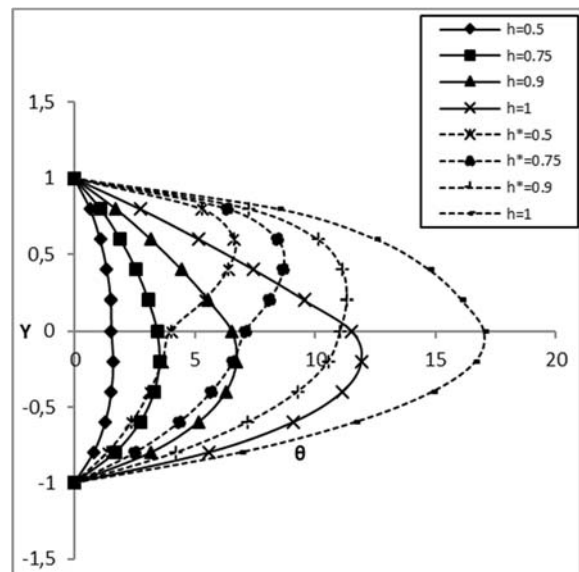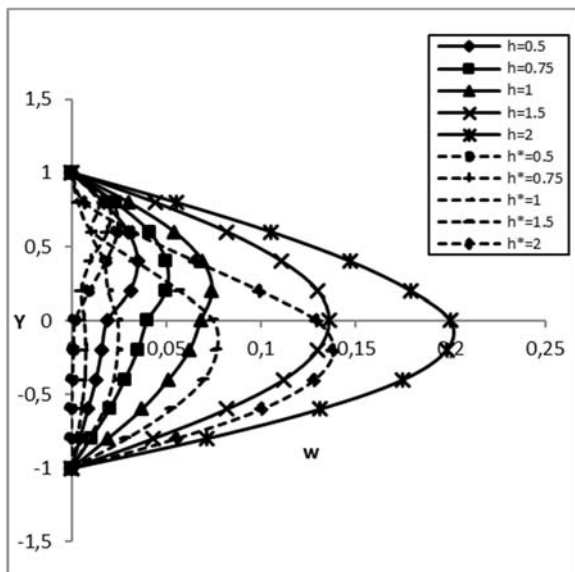
Fig.10 Depicts temperature profiles for unsteady flow (θ_1, θ_2) and the steady case (θ_1^*, θ_2^*) across varying α, with specific parameters:
$h = 0.75, M = 4, m = 2, \sigma_0 = 2, \sigma_{01} = 1.2, \sigma_{02} = 1.5, \varepsilon = 0.5, \rho = 1, t = \pi/\omega, \beta = 0.5, \omega = 1, s = 0.$

Fig.11. Depicts velocity profiles (primary) for unsteady flow (u_1, u_2) and the steady case (u_1^*, u_2^*) across varying h, with specific parameters:
$M = 2, m = 2, \alpha = 0.333, \sigma_0 = 2, \sigma_{01} = 1.2, \sigma_{02} = 1.5, \varepsilon = 0.5, \rho = 1, t = \pi/\omega, \omega = 1, s = 0.$

Fig.12. Depicts velocity profiles (secondary) for unsteady flow (w_1, w_2) and the steady case (w_1^*, w_2^*) across varying h, with specific parameters:
$M = 2, m = 2, \alpha = 0.333, \sigma_0 = 2, \sigma_{01} = 1.2, \sigma_{02} = 1.5, \varepsilon = 0.5, \rho = 1, t = \pi/\omega, \omega = 1, s = 0.$

Fig.13. Depicts temperature profiles for unsteady flow (θ_1, θ_2) and the steady case (θ_1^*, θ_2^*) across varying h, with specific parameters:
$M = 4, m = 2, \alpha = 0.333, \sigma_0 = 2, \sigma_{01} = 1.2, \omega = 1, \sigma_{02} = 1.5, \varepsilon = 0.5, \rho = 1, t = \pi/\omega, \beta = 0.5, s = 0.$
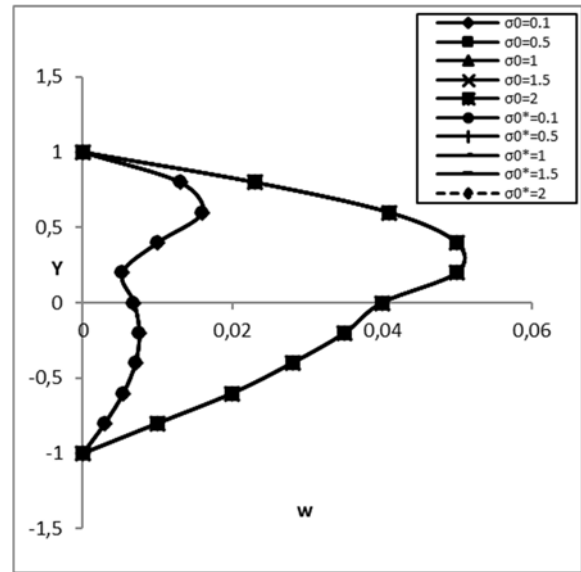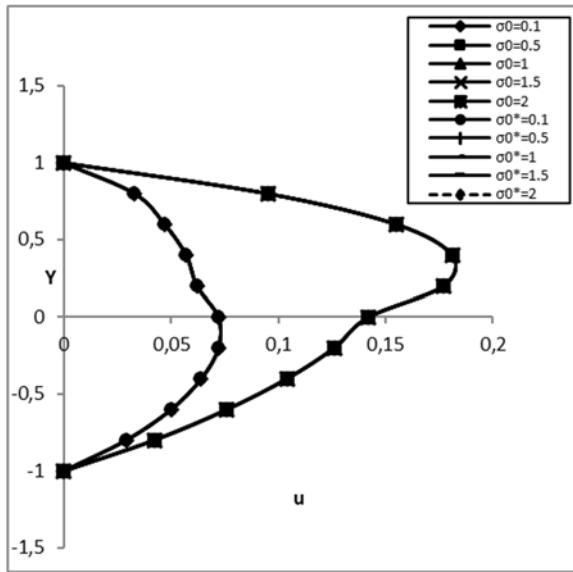
Fig.14. Depicts velocity profiles (primary) for unsteady flow (u_1, u_2) and the steady case (u_1^*, u_2^*) across varying σ_0, with specific parameters: $M = 2$, $m = 2$, $\alpha = 0.333$, $h = 0.75$, $\sigma_{01} = 1.2$, $s = 0$, $\sigma_{02} = 1.5$, $\varepsilon = 0.5$, $\rho = 1$, $t = \pi / \omega$, $\omega = 1$.
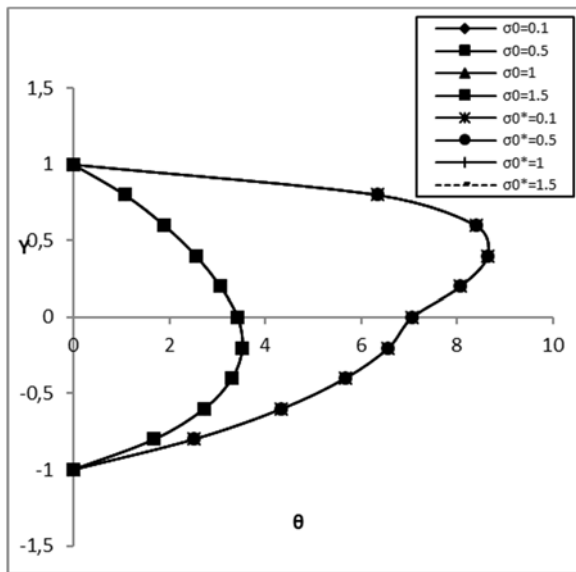

Fig.15. Depicts velocity profiles (secondary) for unsteady flow (w_1, w_2) and the steady case (w_1^*, w_2^*) across varying σ_0, with specific parameters: $M = 2$, $m = 2$, $\alpha = 0.333$, $h = 0.75$, $\sigma_{01} = 1.2$, $s = 0$, $\sigma_{02} = 1.5$, $\varepsilon = 0.5$, $\rho = 1$, $t = \pi / \omega$, $\omega = 1$.

Fig.16. Depicts temperature profiles for unsteady flow (θ_1, θ_2) and the steady case (θ_1^*, θ_2^*) across varying σ_0, with specific parameters: $M = 4$, $m = 2$, $\alpha = 0.333$, $h = 0.75$, $\sigma_{01} = 1.2$, $s = 0$, $\sigma_{02} = 1.5$, $\varepsilon = 0.5$, $\rho = 1$, $t = \pi / \omega$, $\beta = 0.5$, $\omega = 1$.
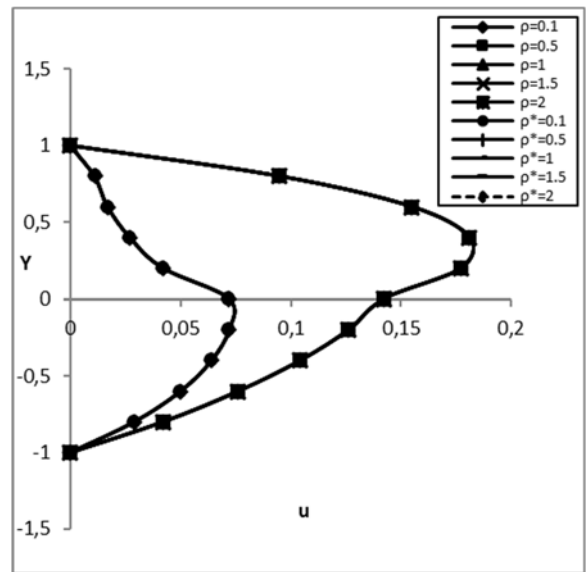

Fig.17. Depicts velocity profiles (primary) for unsteady flow (u_1, u_2) and the steady case (u_1^*, u_2^*) across varying ρ, with specific parameters: $M = 2$, $m = 2$, $\alpha = 0.333$, $h = 0.75$, $\sigma_{01} = 1.2$, $s = 0$, $\sigma_{02} = 1.5$, $\varepsilon = 0.5$, $\sigma_0 = 2$, $t = \pi / \omega$, $\omega = 1$.
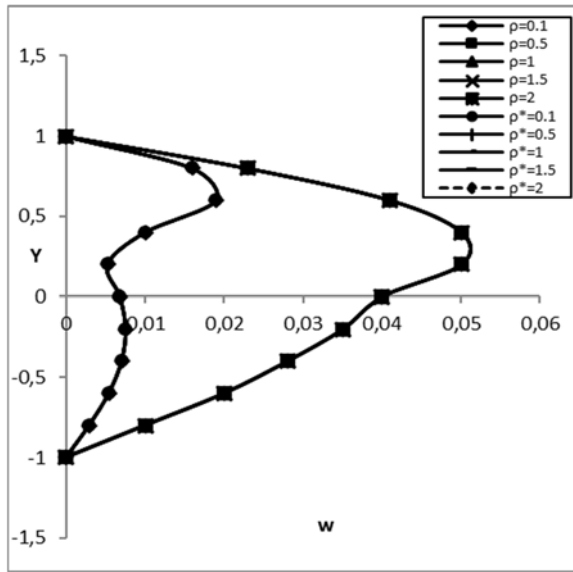
Fig.18. Depicts velocity profiles (secondary) for unsteady flow (w_1, w_2) and the steady case (w_1^*, w_2^*) across varying ρ with specific parameters: $M = 2$, $m = 2$, $\alpha = 0.333$, $h = 0.75$, $\sigma_{01} = 1.2$, $s = 0$, $\sigma_{02} = 1.5$, $\sigma_0 = 2$, $\varepsilon = 0.5$, $t = \pi/\omega$, $\omega = 1$.
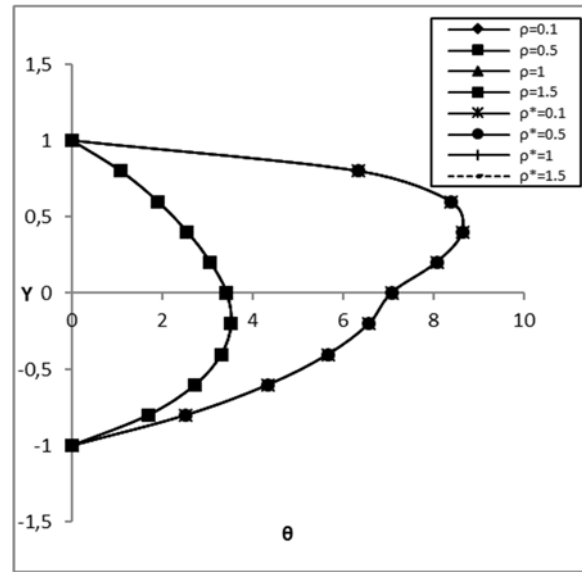

Fig.19. Depicts temperature profiles for unsteady flow (θ_1, θ_2) and the steady case (θ_1^*, θ_2^*) across varying ρ, with specific parameters: $M = 4$, $m = 2$, $\alpha = 0.333$, $h = 0.75$, $\sigma_{01} = 1.2$, $s = 0$, $\sigma_{02} = 1.5$, $\varepsilon = 0.5$, $\sigma_0 = 2$, $t = \pi/\omega$, $\beta = 0.5$, $\omega = 1$.
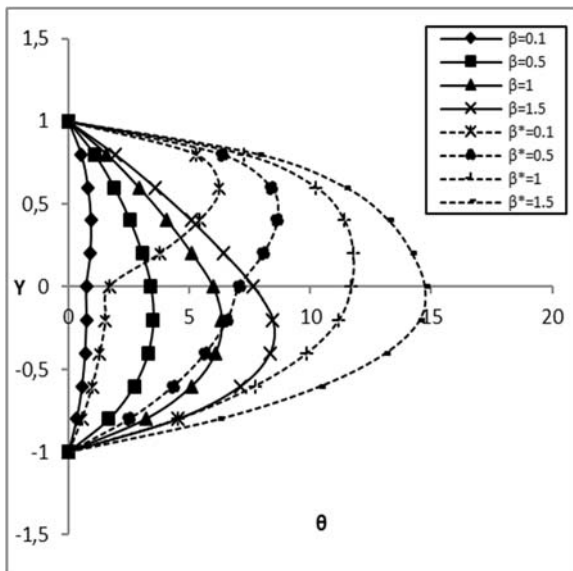

Fig.20. Depicts temperature profiles for unsteady flow (θ_1, θ_2) and the steady case (θ_1^*, θ_2^*) across varying β, with specific parameters: $M = 4$, $m = 2$, $\alpha = 0.333$, $h = 0.75$, $\sigma_{01} = 1.2$, $s = 0$, $\sigma_{02} = 1.5$, $\varepsilon = 0.5$, $\sigma_0 = 2$, $t = \pi/\omega$, $\rho = 1$, $\omega = 1$.
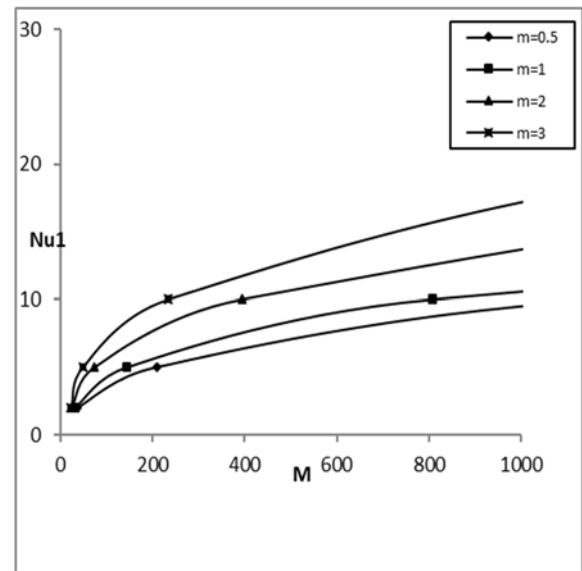

Fig.21. Depicts Nusselt number (Nu_1) is shown across different M values with specific parameters: $h = 0.75$, $m = 2$, $\alpha = 0.333$, $\sigma_0 = 2$, $\sigma_{01} = 1.2$, $s = 0$, $\sigma_{02} = 1.5$, $\varepsilon = 0.5$, $\rho = 1$, $t = \pi/\omega$, $\beta = 0.5$, $\omega = 1$.

The impact of changes in the electrical conductivity ratio σ_0 is illustrated in Figs 14 and 15. It is observed that both primary and secondary velocity distributions show minimal deviation with increasing values of σ_0. As the ratio σ_0 increases, the maximum primary and secondary velocity distributions within the channel tend to shift toward region-I. The effect of modifying the electrical conductivity ratio σ_0 on temperature distribution is portrayed in Fig.16. Notably, there is no significant departure from the temperature distribution as the ratio σ_0 increases in both regions. The highest temperature in the channel tends to migrate towards region-I along the channel centreline with increasing values of σ_0. The outcomes are depicted in Figs 17 and 18, revealing that there is negligible variation in both primary and secondary velocity distributions with incremental changes in ρ. As ρ increases, the primary and secondary velocity distributions within the channel tend to shift towards region-I along the channel centreline. In Fig.19, the influence of changing the densities ratio ρ on temperature distribution in the two fluid regions is showcased. It is determined that there is no significant departure from the temperature distribution as ρ increments occur in both regions. The maximum temperature within the channel tends to move towards region-I along the channel centreline with increasing ρ.

Figure 20 illustrates the impact of the thermal conductivity ratio β on temperature distribution. It is noticed that an increasing β results in an elevation in temperature distribution in both regions. As β increments, the maximum temperature within the channel tends to shift slightly below the channel centreline, moving towards region-II.

Figures 21 and 22 illustrate the heat transfer coefficient rates at the upper and lower plates. Analysis of these figures indicates that, in the scenario where $s = 0$, the heat transfer coefficients at both plates increase with a rise in the Hartmann number M, while maintaining other pertinent parameters constant. Furthermore, it is noted that the heat transfer coefficient rates at the plates show an increase with the escalation of the Hall parameter.
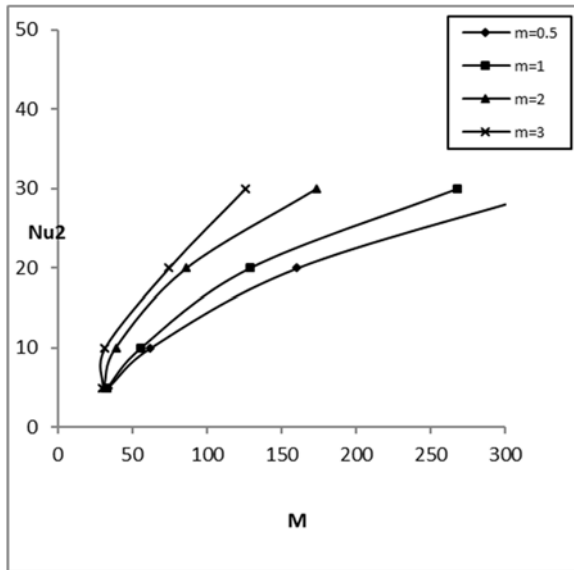

Fig.22. Depicts Nusselt number $\left(Nu_2\right)$ is shown across different M values with specific parameters: $h = 0.75$, $m = 2$, $\alpha = 0.333$, $\sigma_0 = 2$, $\sigma_{01} = 1.2$, $s = 0$, $\sigma_{02} = 1.5$, $\varepsilon = 0.5$, $\rho = 1$, $t = \pi/\omega$, $\beta = 0.5$, $\omega = 1$.
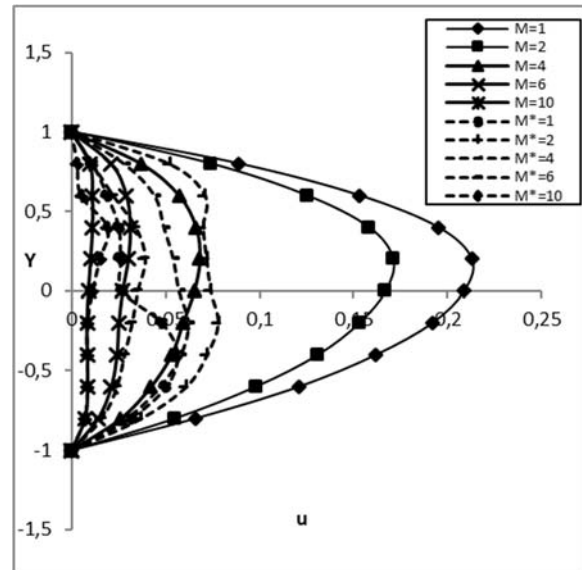
Fig.23. Depicts velocity profiles (primary) for unsteady flow $\left(u_1, u_2\right)$ and the steady case $\left(u_1{}^{*}, u_2{}^{*}\right)$ across varying M, with specific parameters: $h = 0.75$, $m = 2$, $\alpha = 0.9$, $\sigma_0 = 2$, $\sigma_{01} = 1.2$, $s = 0.5$, $\sigma_{02} = 1.5$, $\varepsilon = 0.5$, $\rho = 1$, $t = \pi/\omega$, $\omega = 1$.

In the scenario where the electron-to-total pressure ratio *s* equals (1/2):

The impact of altering the Hartmann number *M* on velocity distributions in two distinct regions is portrayed in Figs 23 and 24. As shown in Fig.23, an increase in *M* results in a reduction of primary velocity distributions in both regions. Conversely, Fig.24 illustrates that an increase in the Hartmann number *M* up to the value of $M = 4$ enhances the secondary velocity distribution, while beyond this value, it decreases in both regions. The maximum primary and secondary velocity distributions in the channel tend to shift above the channel centreline towards region-I as *M* increases. The effect of varying the Hartmann number *M* on temperature distribution is depicted in Fig.25. It is observed that an increase in *M* leads to an augmentation of the temperature distribution in region-I. However, in region-II, the temperature decreases up to $M = 4$, after which it starts increasing. The highest temperature in the channel tends to traverse across the channel centreline towards region-I as *M* increases, with all other governing parameters held constant.
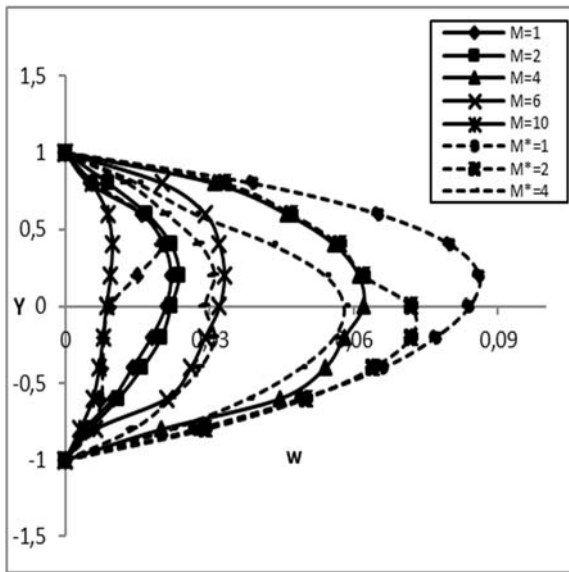

Fig.24. Depicts velocity profiles (secondary) for unsteady flow (w_1, w_2) and the steady case (w_1^*, w_2^*) across varying *M*, with specific parameters: $h = 0.75, m = 2, \alpha = 0.9, \sigma_0 = 2, \sigma_{01} = 1.2, s = 0.5, \sigma_{02} = 1.5, \varepsilon = 0.5, \rho = 1, t = \pi / \omega, \omega = 1.$

Fig.25. Depicts temperature profiles for unsteady flow (θ_1, θ_2) and the steady case (θ_1^*, θ_2^*) across varying *M*, with specific parameters: $h = 0.75, m = 2, \alpha = 0.9, \sigma_0 = 2, \sigma_{01} = 1.2, s = 0.5, \sigma_{02} = 1.5, \varepsilon = 0.5, \rho = 1, t = \pi / \omega, \beta = 0.5, \omega = 1.$
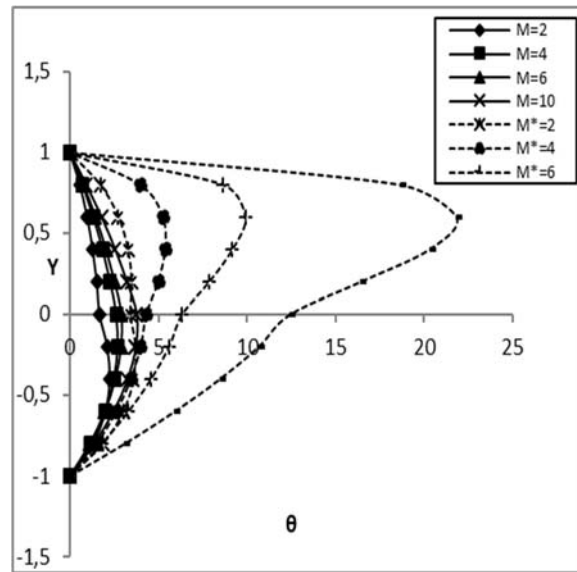
The influence of adjusting the Hall parameter *m* on velocity distributions in two distinct regions is exemplified in Figs 26 and 27. As illustrated in Fig.26, augmenting the parameter *m* leads to a decrease in primary velocity distributions across both regions. In Fig.27, it is observed that an expansion in m up to $m = 1$ enhances the secondary velocity distribution, followed by a decrease in both regions. The maximum secondary velocity distribution in the channel tends to shift above the channel centreline towards region-I as m increases. The impact of varying the Hall parameter *m* on temperature distribution is showcased in Fig.28. It is found that an increase in the Hall parameter *m* leads to a reduction in the temperature distribution in both regions. Furthermore, the highest temperature distribution in the channel tends to move above the channel centreline towards region-I as *m* increases.

The impact of the viscosity ratio, denoted as α, is illustrated in Figs 29 and 30. It is evident that an augmentation in α enhances both primary and secondary velocity distributions across the two regions. With increasing α, the peak primary velocity distribution within the channel tends to shift above the centreline

towards region-I, while the peak secondary velocity distribution tends to shift below the centreline towards region-II. The influence of the viscosity ratio α on temperature distribution is depicted in Fig.31. It is noteworthy that an increase in α raises the temperature distribution up to $\alpha = 0.5$, beyond which it diminishes in both regions. Moreover, the temperature distribution within the channel tends to shift below the centreline towards region-II as α increases.
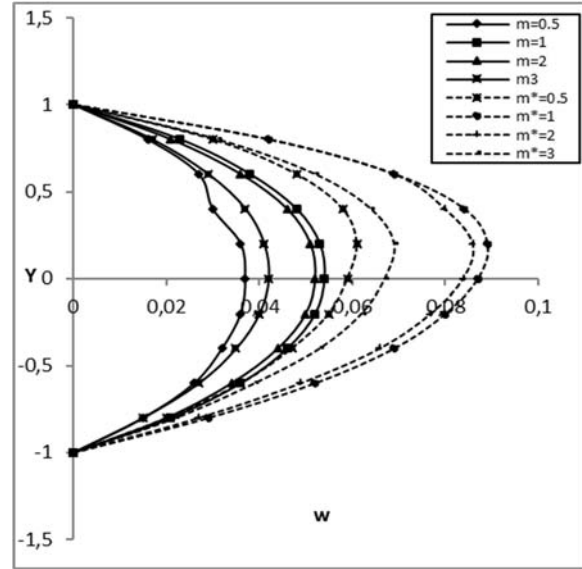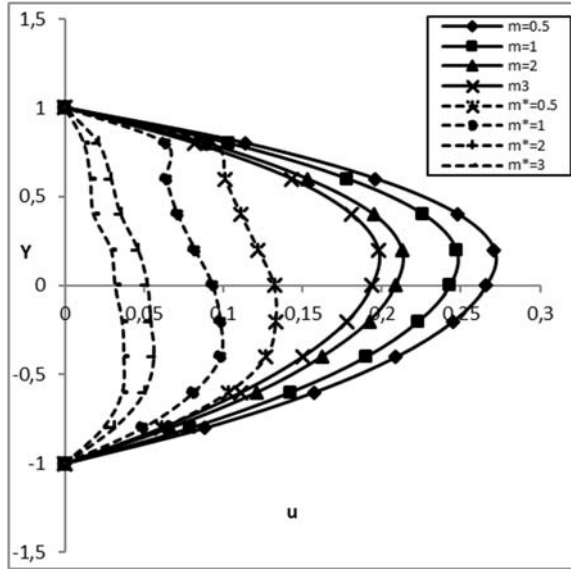

Fig.26. Depicts velocity profiles (primary) for unsteady flow (u_1, u_2) and the steady case (u_1^*, u_2^*) across varying m, with specific parameters: $h = 0.75, M = 1$, $\alpha = 0.9$, $\sigma_0 = 2$, $\sigma_{01} = 1.2$, $s = 0.5$, $\sigma_{02} = 1.5$, $\varepsilon = 0.5$, $\rho = 1$, $t = \pi / \omega$, $\omega = 1$.

Fig.27. Depicts velocity profiles (secondary) for unsteady flow (w_1, w_2) and the steady case (w_1^*, w_2^*) across varying m, with specific parameters: $h = 0.75, M = 1$, $\alpha = 0.9$, $\sigma_0 = 2$, $\sigma_{01} = 1.2$, $s = 0.5$, $\sigma_{02} = 1.5$, $\varepsilon = 0.5$, $\rho = 1$, $t = \pi / \omega$, $\omega = 1$.

The impact of the height ratio h on both primary and secondary velocity distributions is illustrated in Figs 32 and 33. Fig.32 demonstrates that an increase in h enhances the primary velocity distribution in both regions. However, Fig.33 depicts that an increment in h up to $h = 1$ amplifies the secondary velocity distribution, followed by a decrease in both regions. The maximum primary and secondary velocity distributions in the channel tend to shift below the channel centreline towards region-II as h increases. The influence of varying the height ratio h on temperature distribution is presented in Fig.34. It is observed in both regions that an increase in h leads to an enhancement in the temperature distribution. Furthermore, the highest temperature in the channel tends to move below the channel centreline towards region-II as h increments.

The impact of the electrical conductivity ratio σ_0 is depicted in Figs 35 and 36. It is observed that an increase in σ_0 amplifies both primary and secondary velocity distributions in the two regions. As σ_0 increases, the maximum primary velocity distribution in the channel tends to shift above the channel centreline towards region-I, while the maximum secondary velocity distribution tends to move below the channel centreline towards region-II. The influence of varying the electrical conductivity ratio σ_0 on temperature distribution is illustrated in Fig.37. It is found that an increase in σ_0 enhances the temperature distribution in both regions. The highest temperature distribution in the channel tends to shift over the channel centerline towards region-I as σ_0 increments.
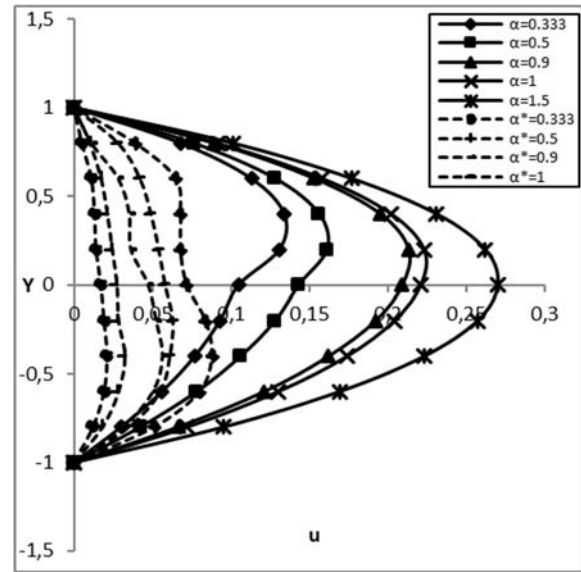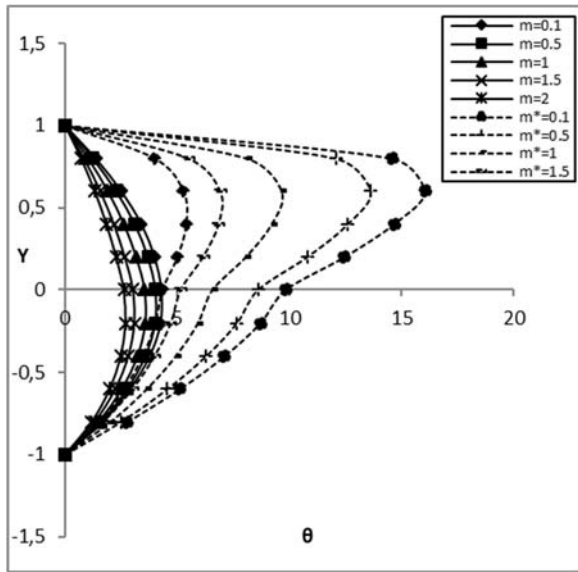
Fig.28.Depicts temperature profiles for unsteady flow (θ_1, θ_2) and the steady case (θ_1^*, θ_2^*) across varying m, with specific parameters: $h = 0.75, M = 1, \alpha = 0.9, \sigma_0 = 2, \sigma_{01} = 1.2, s = 0.5, \sigma_{02} = 1.5, \varepsilon = 0.5, \rho = 1, t = \pi / \omega, \beta = 0.5, \omega = 1.$

Fig.29.Depicts velocity profiles (primary) for unsteady flow (u_1, u_2) and the steady case (u_1^*, u_2^*) across varying α, with specific parameters: $h = 0.75, M = 1, m = 2, \sigma_0 = 2, \sigma_{01} = 1.2, s = 0.5, \sigma_{02} = 1.5, \varepsilon = 0.5, \rho = 1, t = \pi / \omega, \omega = 1.$

Fig.30.Depicts velocity profiles (secondary) for unsteady flow (w_1, w_2) and the steady case (w_1^*, w_2^*) across varying α, with specific parameters: $h = 0.75, M = 1, m = 2, \sigma_0 = 2, \sigma_{01} = 1.2, s = 0.5, \sigma_{02} = 1.5, \varepsilon = 0.5, \rho = 1, t = \pi / \omega, \omega = 1.$
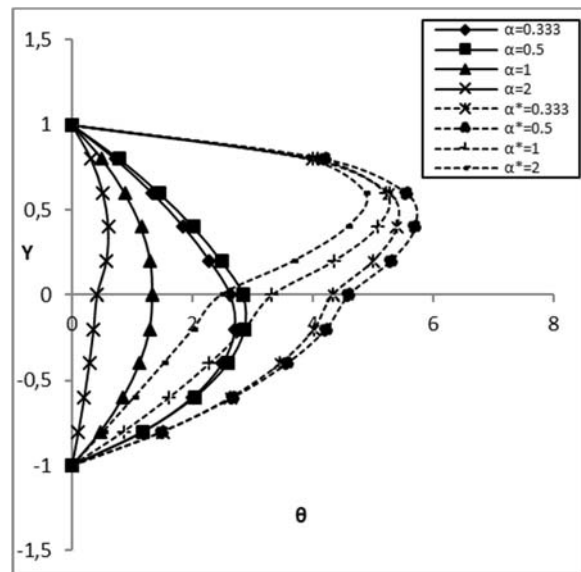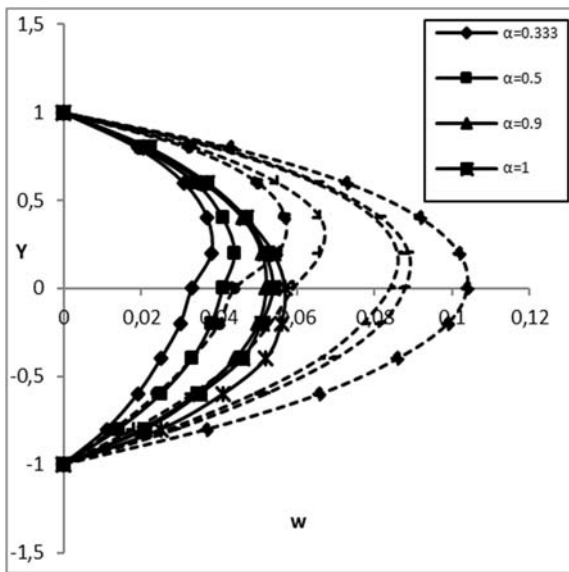

Fig.31.Depicts temperature profiles for unsteady flow (θ_1, θ_2) and the steady case (θ_1^*, θ_2^*) across varying α, with specific parameters: $h = 0.75, M = 1, m = 2, \sigma_0 = 2, \sigma_{01} = 1.2, \sigma_{02} = 1.5, \varepsilon = 0.5, \rho = 1, t = \pi / \omega, \beta = 0.5, \omega = 1, s = 0.5.$
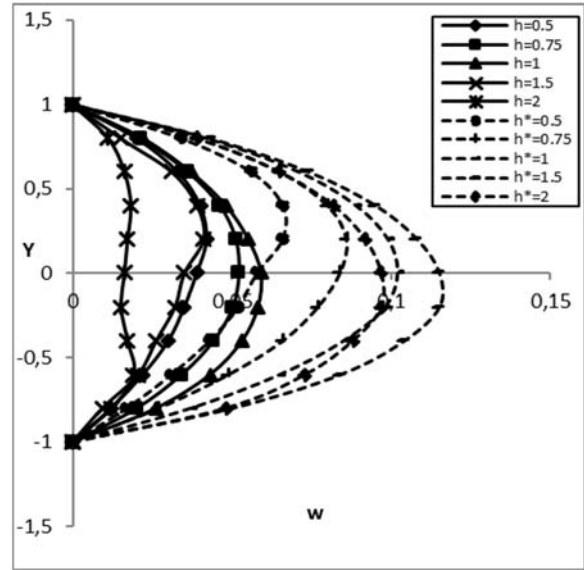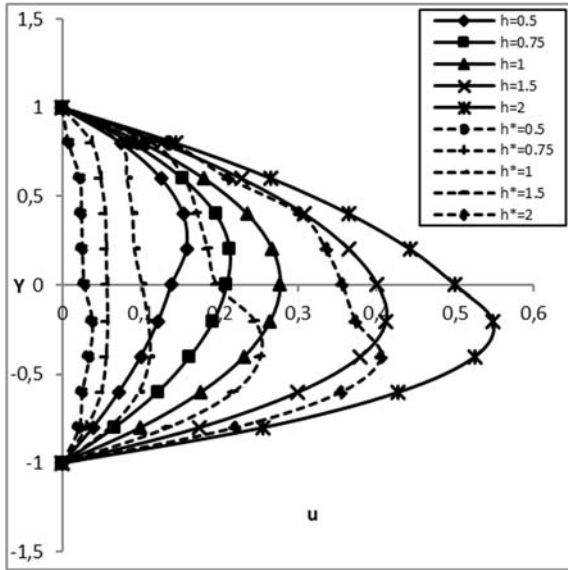
Fig.32.Depicts velocity profiles (primary) for unsteady flow $\left(u_1,u_2\right)$ and the steady case $\left(u_1^*,u_2^*\right)$ across varying h, with specific parameters: $M = 1$, $m = 2$, $\alpha = 0.9$, $\sigma_0 = 2$, $\sigma_{01} = 1.2$, $\sigma_{02} = 1.5$, $\varepsilon = 0.5$, $\rho = 1$, $t = \pi / \omega$, $\omega = 1$, $s = 0.5$.

Fig.33.Depicts velocity profiles (secondary) for unsteady flow $\left(w_1,w_2\right)$ and the steady case $\left(w_1^*,w_2^*\right)$ across varying h, with specific parameters: $M = 1$, $m = 2$, $\alpha = 0.9$, $\sigma_0 = 2$, $\sigma_{01} = 1.2$, $\sigma_{02} = 1.5$, $\varepsilon = 0.5$, $\rho = 1$, $t = \pi / \omega$, $\omega = 1$, $s = 0.5$.

Fig.34.Depicts temperature profiles for unsteady flow $\left(\theta_1,\theta_2\right)$ and the steady case $\left(\theta_1^*,\theta_2^*\right)$ across varying h, with specific parameters: $M = 1$, $m = 2$, $\alpha = 0.9$, $\sigma_0 = 2$, $\sigma_{01} = 1.2$, $\sigma_{02} = 1.5$, $\varepsilon = 0.5$, $\rho = 1$, $t = \pi / \omega$, $\beta = 0.5$, $\omega = 1$, $s = 0.5$.

Fig.35.Depicts velocity profiles (primary) for unsteady flow $\left(u_1,u_2\right)$ and the steady case $\left(u_1^*,u_2^*\right)$ across varying σ_0 , with specific parameters: $M = 1$, $m = 2$, $\alpha = 0.9$, $h = 0.75$, $\sigma_{01} = 1.2$, $\sigma_{02} = 1.5$, $\varepsilon = 0.5$, $\rho = 1$, $t = \pi / \omega$, $\omega = 1$, $s = 0.5$.

Fig.36.Depicts velocity profiles (secondary) for unsteady flow $\left(w_1, w_2\right)$ and the steady case $\left(w_1^*, w_2^*\right)$ across varying σ_0, with specific parameters: $M = 1, m = 2, \alpha = 0.9, h = 0.75, \sigma_{01} = 1.2, \sigma_{02} = 1.5, \varepsilon = 0.5, \rho = 1, t = \pi / \omega, \omega = 1, s = 0.5.$
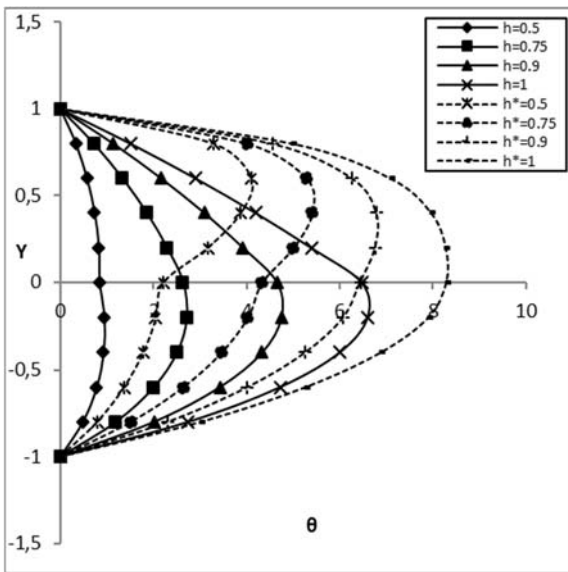
Fig.37.Depicts temperature profiles for unsteady flow $\left(\theta_1, \theta_2\right)$ and the steady case $\left(\theta_1^*, \theta_2^*\right)$ across varying σ_0, with specific parameters: $M = 1, m = 2, \alpha = 0.9, h = 0.75, \sigma_{01} = 1.2, \sigma_{02} = 1.5, \varepsilon = 0.5, \rho = 1, t = \pi / \omega, \beta = 0.5, \omega = 1, s = 0.5.$
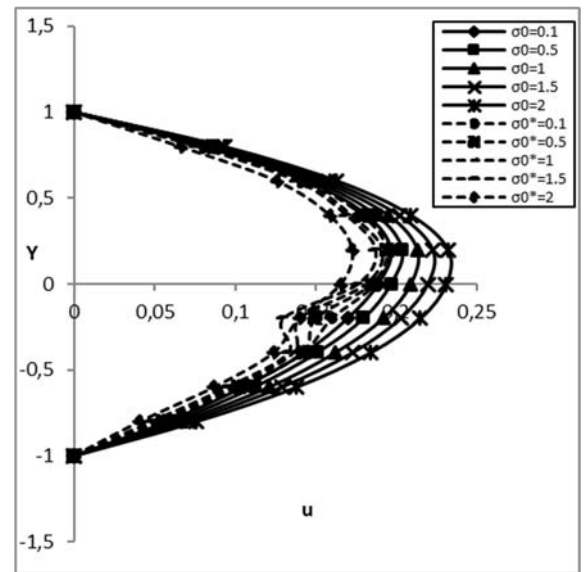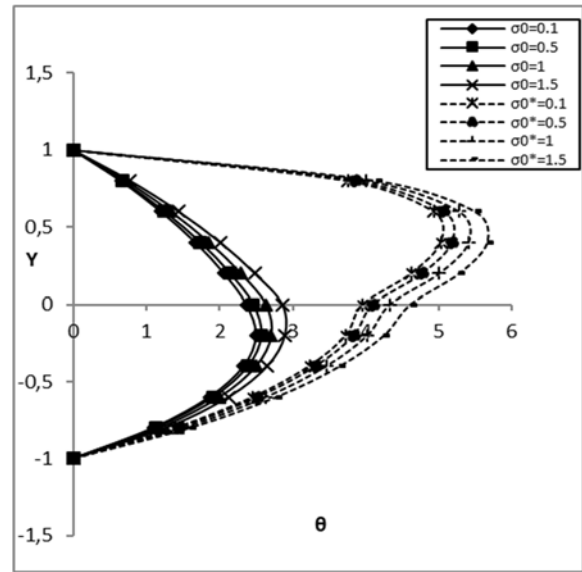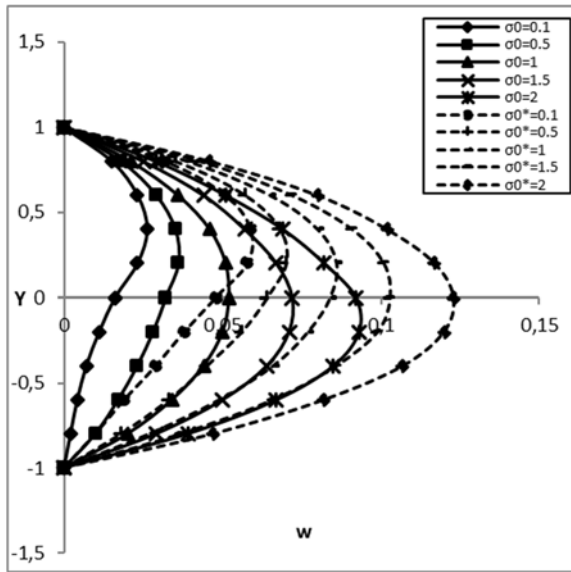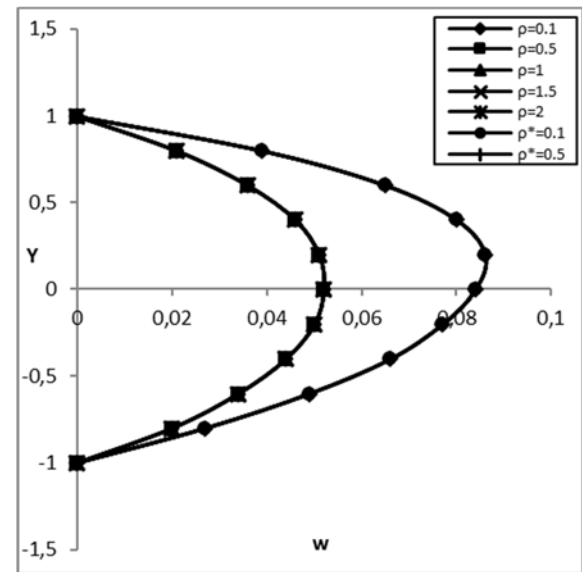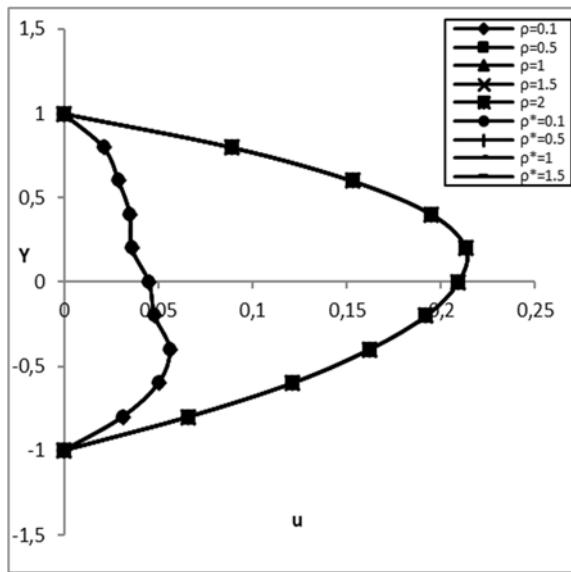
Fig.38.Depicts velocity profiles (primary) for unsteady flow $\left(u_1, u_2\right)$ and the steady case $\left(u_1^*, u_2^*\right)$ across varying ρ, with specific parameters: $M = 1, m = 2, \alpha = 0.9, h = 0.75, \sigma_{01} = 1.2, \sigma_{02} = 1.5, \varepsilon = 0.5, \sigma_0 = 2, t = \pi / \omega, \omega = 1, s = 0.5.$

Fig.39.Depicts velocity profiles (secondary) for unsteady flow $\left(w_1, w_2\right)$ and the steady case $\left(w_1^*, w_2^*\right)$ across varying ρ with specific parameters: $M = 1, m = 2, \alpha = 0.9, h = 0.75, \sigma_{01} = 1.2, \sigma_{02} = 1.5, \sigma_0 = 2, \varepsilon = 0.5, t = \pi / \omega, \omega = 1, s = 0.5.$
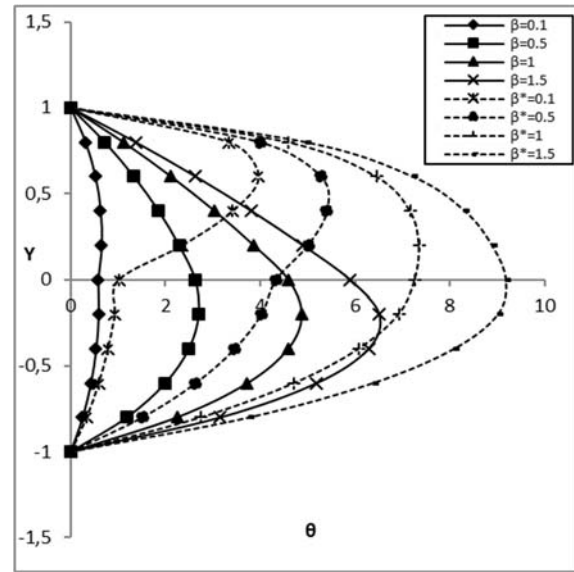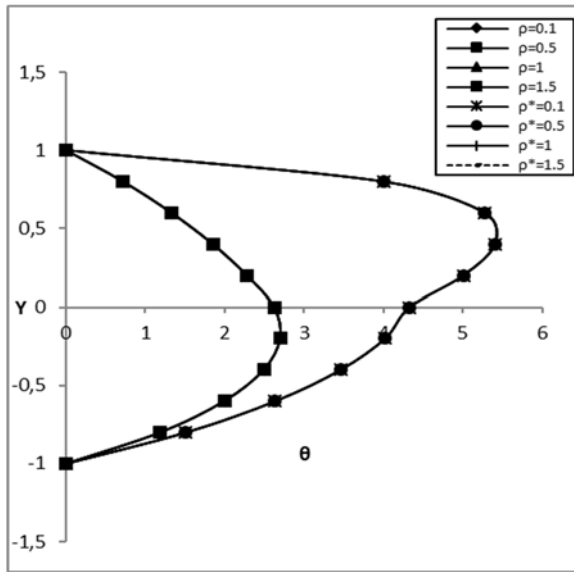
Fig.40. Depicts temperature profiles for unsteady flow $\left(\theta_1, \theta_2\right)$ and the steady case $\left(\theta_1^*, \theta_2^*\right)$ across varying ρ, with specific parameters: $M = 1$, $m = 2$, $\alpha = 0.9$, $h = 0.75$, $\sigma_{01} = 1.2$, $\sigma_{02} = 1.5$, $\varepsilon = 0.5$, $\sigma_0 = 2$, $t = \pi / \omega$, $\beta = 0.5$, $\omega = 1$, $s = 0.5$.

Fig.41. Depicts temperature profiles for unsteady flow $\left(\theta_1, \theta_2\right)$ and the steady case $\left(\theta_1^*, \theta_2^*\right)$ across varying β, with specific parameters: $M = 1$, $m = 2$, $\alpha = 0.9$, $h = 0.75$, $\sigma_{01} = 1.2$, $\sigma_{02} = 1.5$, $\varepsilon = 0.5$, $\sigma_0 = 2$, $t = \pi / \omega$, $\rho = 1$, $\omega = 1$, $s = 0.5$.
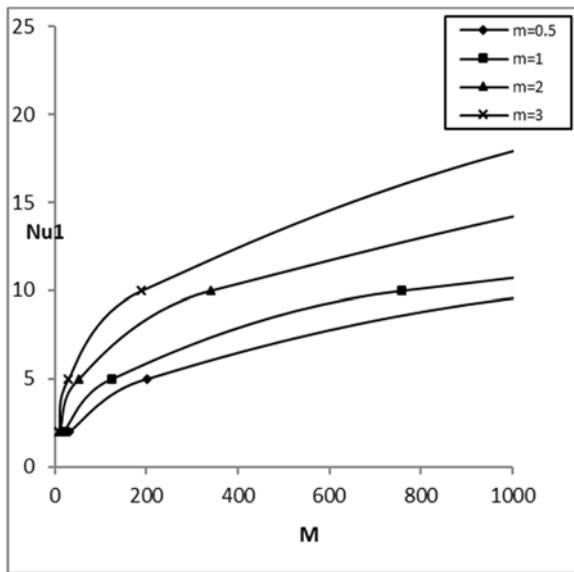
Fig.42. Depicts Nusselt number $\left(Nu_1\right)$ is shown across different M values with: $h = 0.75$, $m = 2$, $\alpha = 0.9$, $\sigma_0 = 2$, $\sigma_{01} = 1.2$, $\sigma_{02} = 1.5$, $\varepsilon = 0.5$, $\rho = 1$, $t = \pi / \omega$, $\beta = 0.5$, $\omega = 1$, $s = 0.5$.


Fig.43. Depicts Nusselt number $\left(Nu_2\right)$ is shown across different M values with: $h = 0.75$, $m = 2$, $\alpha = 0.9$, $\sigma_0 = 2$, $\sigma_{01} = 1.2$, $\sigma_{02} = 1.5$, $\varepsilon = 0.5$, $\rho = 1$, $t = \pi / \omega$, $\beta = 0.5$, $\omega = 1$, $s = 0.5$.

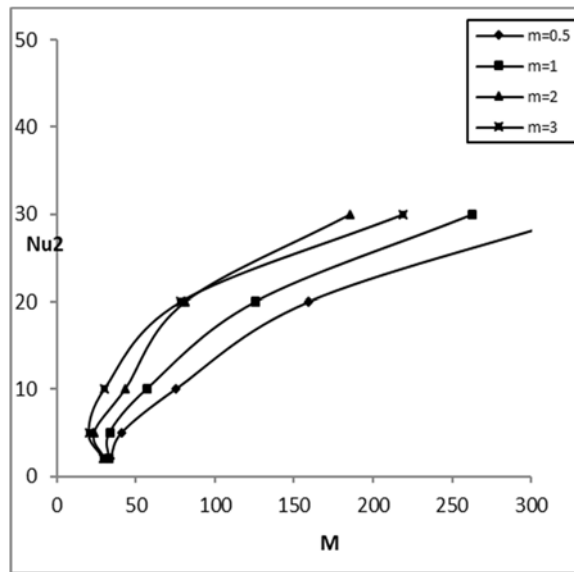The importance of ρ is illustrated in Figs 38 and 39. It is observed that there is no significant deviation in both primary and secondary velocity distributions as ρ increases. The maximum primary and secondary

velocity distributions in the channel tend to shift over the channel centreline towards region-I as ρ increments. Figure 40 portrays the impact of ρ representing the ratio of densities, on temperature distribution in the two fluid regions. It is found that there is no notable departure from the temperature distribution as ρ increases in both regions. As the parameter ρ increases, the peak temperature within the channel exhibits a tendency to shift along the channels central axis towards region-I.

Figure 41 depicts the influence of the thermal conductivity ratio β on temperature distribution. It is observed that an increase in β leads to an elevation of the temperature distribution in both regions. As β increments, the highest temperature in the channel tends to shift slightly below the channel centreline towards region-II.

Figures 42 and 43 depict the heat transfer coefficients at both plates plotted against the Hartmann number, considering the condition when $s = 1/2$. Analysis of these figures indicates that an increase in the Hartmann number results in an augmentation of the heat transfer coefficients, assuming all other governing parameters remain constant. Furthermore, it is observed that an increase in the Hall parameter also enhances the heat transfer coefficients under the condition where all other governing parameters are held fixed.

5. Conclusions

When the lateral plates are made of conductive material, an exploration into the effects of Hall currents on the magnetohydrodynamic (MHD) flow of two liquid substances in an unsteady manner through plasma is carried out in a straight channel bounded by infinitely long plates. The solutions for the velocity and temperature fields in the two liquid zones depend solely on the electron pressure to total pressure ratio. The study delves into the influence of various factors such as the Hartmann number, Hall parameter, as well as viscosities, densities, heights, electrical conductivities, and thermal conductivity ratios on the velocity and temperature distributions within the two liquid zones. The investigation employs distribution profiles for two distinct scenarios, one with a zero ionization parameter and another with a half ionization parameter. The principal research findings are summarized as follows for both cases:

In the scenario where the electron-to-total pressure ratio (s) is zero:

- Higher Hartmann number decreases temperature distribution in both regions.
- Hall parameter rise expands temperature distribution in region-II but reduces it in region-I after reaching a specific value.
- Rise in height ratio, viscosity ratio, or electrical conductivity improves both primary and secondary velocity distributions in both regions.
- Temperature distribution rises with an increase in height ratio or thermal conductivity ratio in both regions.
- Heat transfer coefficients at both plates increase with higher Hartmann numbers and Hall parameters, keeping other parameters constant.

In the scenario where the electron-to-total pressure ratio (s) is 1/2:

- Hartmann number decreases primary velocity distribution in both regions while increases temperature distribution in region-I.
- Hall parameter decreases temperature distribution in both regions.
- Viscosity and electrical conductivity ratio influence the velocity distributions.
- Temperature rises with the increase of height, electrical, or thermal ratios.
- The heat transfer coefficients increase with higher Hartmann number and Hall parameter, with other parameters constant.

Acknowledgements

Nomenclature

$\left.\begin{array}{l} A_1, A_2, ...a_1, a_2, .. \\ B_1, B_2, ...b_1, b_2, ... \end{array}\right\}$ − mathematical symbols or functional relations featured in the equations and solutions

$\overline{B}$ − magnetic flux density $[T]$

B_0 − application of a uniform transverse magnetic field $[A/m]$

E_x, E_z − application of electric fields in the x- and z-directions, respectively $[V/m]$

e − electric charge $[C]$

h − ratio of the heights of the two regions

h_1 − height of the channel in the upper region (Region-I)

h_2 − height of the channel in the lower region (Region-II)

$I_{x_1}, I_{z_1}; I_{x_2}, I_{z_2}$ − dimensionless current densities along the x- and z-directions in two fluid regions

J_x, J_z − current densities in the x- and z-directions, respectively

$\overline{J}$ − current density $[A/cm^2]$

K_1, K_2 − thermal conductivities of the two fluids in Region-I and Region-II $[W/(mK)]$

M − Hartmann number

m − Hall parameter $[m^2/C]$

$m_1, m_2, m_3, ...$ − symbols or functional relationships taken into account in the equations and solutions

m_x, m_z − dimensionless electric fields

N_1, N_2 − symbols represented as $N_1 = m_{x_1} + im_{z_1}$ and $N_2 = m_{x_2} + im_{z_2}$

Nu_1, Nu_2 − rate of heat transfer coefficients at upper and lower plates, respectively $[W/(m^2 K)]$

P − pressure $[Pa]$

p_e − electron pressure $[Pa]$

Pr − Prandtl number

$q_{01}, q_{02}, q_{11}, q_{12}$ − use of complex notations for simplicity

q_{m_1}, q_{m_2} − complex form of the mean velocities $[m/s]$

s − $= pe/p$ (ratio of electron pressure to the total pressure)

t, T − time, temperature $[s], [K]$

T_{w_1}, T_{w_2} − constant plate temperatures

U_1, U_2 − symbols used for simplicity as $U_1 = q_1/q_{m_1}, U_2 = q_2/q_{m_2}$

$\overline{U_1}, \overline{U_2}$ − complex conjugates of U_1, U_2

u_1, u_2 − primary velocity distributions in the two fluid regions

u_{m_1}, u_{m_2} − primary mean velocity distributions in the two fluid regions

$u_{01}(y), u_{02}(y)$ − primary velocity distributions in the steady-state case in two fluid regions

$u_{11}(y), u_{12}(y)$ − transient primary velocity components in the two fluid regions

u_p − $\left(-\dfrac{\partial p}{\partial x}\dfrac{h_1^2}{\rho_1 \nu_1}\right)$, characteristic velocity

w_1, w_2 − secondary velocity distributions in the two fluid regions

w_{m_1}, w_{m_2} − secondary mean velocity distributions in the two fluid regions

$w_{01}(y), w_{02}(y)$ − secondary velocity distributions in the steady-state case in two regions

$w_{11}(y), w_{12}(y)$ − transient secondary velocity components in two regions

(x, y, z) − space coordinates

α − ratio of viscosities

β − ratio of thermal conductivities

μ_1, μ_2 − viscosities of the two fluids $[Pa\ s]$

σ_0 − ratio of electrical conductivities

σ_1, σ_2 − modified conductivities parallel and normal to the direction of the electric field

σ_{01}, σ_{02} − electrical conductivities of the two fluids $[S/m]$

$\sigma_{11}, \sigma_{12}, \sigma_{21}, \sigma_{22}$ − modified conductivities parallel and normal to the direction of the electric field

ε − amplitude (a small constant quantity, $\varepsilon \ll 1$) $[m/s]$

ρ − ratio of densities

ρ_0 − free charge density $\left[C/m^2\right]$

ρ_1, ρ_2 − densities of the two fluids $\left[kg/m^2\right]$

θ_1, θ_2 − non-dimensional forms of temperature distributions of the two fluids

$\theta_{01}(y), \theta_{02}(y)$ − temperature distributions under the steady state in the two regions $[K]$

$\theta_{11}(y), \theta_{12}(y)$ − temperature distributions under transient state in the two fluid regions

τ, τ_e − mean collision time between electron and ion, electron and neutral particles

ω − frequency of oscillation $[Hz]$

Appendix

$$\beta_1 = 1 - s\left(\frac{1}{1+m^2}\right), \quad \beta_2 = \frac{-sm}{1+m^2}, \quad \beta_3 = 1 - s\left(1 - \frac{\sigma_0\sigma_{01}}{1+m^2}\right), \quad \beta_4 = \frac{-s\sigma_0\sigma_{02}m}{1+m^2}, \quad D_1 = \beta_1 + i\beta_2, \quad D_2 = \beta_3 + i\beta_4,$$

$$D_3 = i\sigma_1 + m\sigma_2, \quad N_1 = m_{1x} + i\,m_{1z}, \quad N_2 = m_{2x} + im_{2z}, \quad a_1 = \frac{M^2}{1+mi}, \quad a_2 = -\left(D_1 + \frac{M^2 N_1}{m-i}\right),$$

$$a_3 = \left(\frac{\alpha h^2 M^2 D_3}{1+m^2}\right), \quad a_4 = -\left(D_2 \alpha h^2 + \frac{\alpha h^2 M^2 N_2 D_3}{1+m^2}\right), \quad m_1 = \sqrt{a_1}, \quad m_2 = -\sqrt{a_1}, \quad m_3 = \sqrt{a_3}, \quad m_4 = -\sqrt{a_3},$$

$$m_5 = \sqrt{(a_1 - \omega \tan \omega t)}, \quad m_6 = -\sqrt{(a_1 - \omega \tan \omega t)}, \quad m_7 = \sqrt{(a_3 - \omega \tan \omega t)}, \quad m_8 = -\sqrt{(a_3 - \omega \tan \omega t)},$$

$$a_{97} = \frac{e^{m_1} - 1}{m_1}, \quad a_{98} = \frac{e^{m_2} - 1}{m_2}, \quad a_{99} = \frac{e^{m_3} - 1}{m_3}, \quad a_{100} = \frac{e^{m_4} - 1}{m_4}, \quad A_1 = a_5 a_8 + a_{11} a_9,$$

$$A_2 = \frac{e^{m_2} D_1 + M^2 N_1 (i+m)}{M^2 (mi - 1)} - A_1 e^{m_1 - m_2}, \quad A_3 = \frac{a_8 + A_1 \left(1 - e^{m_1 - m_2}\right)}{1 - e^{-m_3 + m_4}},$$

$$A_4 = \frac{-e^{m_4}\left\{D_2 \alpha h^2 \left(1 + m^2\right) + \alpha h^2 M^2 N_2 D_3\right\}}{\alpha h^2 M^2 D_3} - A_3 e^{-m_3 + m_4}, \quad A_5 = \frac{e^{-m_2} D_1 (mi + 1)}{M^2},$$

$$A_6 = \frac{e^{-m_6}\left\{M^2 + e^{m_2 + m_5} D_1 (mi + 1)\right\}}{M^2}, \quad A_7 = \frac{e^{-m_7}\left\{M^2 + e^{m_3 + m_6} D_2 (mi + 1)\right\}}{M^2}, \quad A_8 = \frac{-m e^{-m_2}}{(mi - 1)},$$

$$A_{28} = \frac{\varepsilon \cos \omega t \left\{a_7 m_5 \left(e^{m_4} - 1\right) + \left(m_4 m_5 - m_5 m_6 e^{-m_2 + m_3}\right)\left(e^{m_5} - 1\right)\right\}}{\alpha h m_4 m_5},$$

$$A_{29} = \frac{\varepsilon \cos \omega t \left\{a_8 m_7 \left(e^{m_6} - 1\right) + m_2 - m_3 m_6 e^{m_2 - m_3}\left(e^{m_7} - 1\right)\right\}}{m_6 m_7},$$

$$B_9 = b_{289}, \quad B_{10} = -b_{279} - b_{289}, \quad B_{11} = b_{288}, \quad B_{12} = -b_{280} + b_{288}, \quad B_{13} = b_{345} b_{217} + b_{335}, \quad B_{14} = b_{345},$$

$$B_{15} = b_{344} b_{219} + b_{336}, \quad B_{16} = b_{344}, \quad b_{23} = \frac{M^2 m_2^2 A_2 \left(\overline{a_2} + \overline{q_{m_1}} \overline{a_1}\right)}{\left(1 + m^2\right) q_{m_1} \overline{q_{m_1}} \overline{a_1}}, \quad b_{24} = \frac{M^2 \overline{A_1} m_1^2 \left(a_2 + q_{m_1} a_1\right)}{\left(1 + m^2\right) a_1 q_{m_1} \overline{q_{m_1}}},$$

$$b_{25} = \frac{M^2 \overline{A_2 m_2}^2 \left(a_2 - q_{m_1} a_1\right)}{\left(1 + m^2\right) a_1 q_{m_1} \overline{q_{m_1}}}, \quad b_{26} = \frac{-2M^2 \left\{\overline{a_2}\left(a_2 + a_1 q_{m_1}\right) + a_1 \overline{a_1}\left(\overline{q_{m_1}} a_2 + q_{m_1} \overline{q_{m_1}}\right)\right\}}{\left(1 + m^2\right) a_1 \overline{a_1} q_{m_1} \overline{q_{m_1}}}, \quad b_{75} = m_3 + \overline{m_4},$$

$$b_{76} = m_4 + \overline{m_3}, \quad b_{77} = m_4 + \overline{m_4}, \quad b_{78} = b_{57} + b_{61}, \quad b_{79} = b_{58} + b_{62}, \quad b_{120} = \sqrt{b_{114} / b_{113}}, \quad b_{94} = \frac{b_{86}}{b_{74}},$$

$$b_{95} = \frac{b_{87}}{b_{75}}, \quad b_{96} = \frac{b_{88}}{b_{76}}, \quad b_{97} = \frac{b_{89}}{b_{77}}, \quad b_{138} = m_5 + \overline{m_5}, \quad b_{139} = m_5 + \overline{m_6}, \quad b_{140} = m_6 + \overline{m_5},$$

$$b_{141} = m_6 + \overline{m_6}, \quad b_{146} = \frac{b_{142}}{b_{138}^2 - b_{120}^2}, \quad b_{147} = \frac{b_{143}}{b_{139}^2 - b_{120}^2}, \quad b_{148} = \frac{b_{144}}{b_{140}^2 - b_{120}^2}, \quad b_{149} = \frac{b_{145}}{b_{141}^2 - b_{120}^2},$$

$$b_{185} = m_7 + \overline{m_7}, \quad b_{186} = m_7 + \overline{m_8}, \quad b_{187} = m_8 + \overline{m_7}, \quad b_{188} = m_8 + \overline{m_8}, \quad b_{251} = \frac{b_{245}}{b_{23}}, \quad b_{252} = \frac{b_{246}}{b_{24}},$$

$$b_{253} = \frac{b_{238}}{b_{25}}, \quad b_{254} = \frac{b_{247}}{m_1}, \quad b_{255} = \frac{b_{248}}{m_2}, \quad b_{256} = \frac{b_{249}}{m_1}, \quad b_{257} = \frac{b_{250}}{m_2}, \quad b_{258} = -\frac{b_{244}}{2}, \quad b_{274} = \frac{b_{270}}{m_3},$$

$$b_{275} = \frac{b_{271}}{m_4}, \quad b_{276} = \frac{b_{272}}{m_3}, \quad b_{277} = \frac{b_{273}}{m_4}, \quad b_{278} = -\frac{b_{263}}{2}, \quad b_{297} = \frac{b_{293}}{\left(\overline{m_5}\right)^2 - b_{120}{}^2}, \quad b_{298} = \frac{b_{294}}{\left(\overline{m_6}\right)^2 - b_{120}{}^2},$$

$$b_{299} = \frac{b_{295}}{m_5{}^2 - b_{120}{}^2}, \quad b_{300} = \frac{b_{296}}{m_6{}^2 - b_{120}{}^2}, \quad b_{317} = \frac{b_{315}}{b_{185}{}^2 - b_{120}{}^2}, \quad b_{318} = \frac{b_{316}}{b_{186}{}^2 - b_{120}{}^2},$$

$$b_{319} = \frac{b_{311}}{m_7{}^2 - b_{120}{}^2}, \quad b_{320} = \frac{b_{312}}{m_8{}^2 - b_{120}{}^2}, \quad b_{321} = \frac{b_{313}}{\left(\overline{m_7}\right)^2 - b_{120}{}^2}, \quad b_{322} = \frac{b_{314}}{\left(\overline{m_8}\right)^2 - b_{120}{}^2}.$$

References

[1] Shail R. (1973): *On laminar two-phase flows in magnetohydrodynamics.*– Int. J. Engg. Sci., vol.11, pp.1103-1109.

[2] Cowling T.G.(1962):*Magnetohydrodynamics.*– Rep. Prog. Phys., vol.25, pp.244.

[3] Hall Edwin (1879): *On a new action of the magnet on electric currents.*– American Journal of Mathematics, vol.2, No.2, pp. 287-292.

[4] Broer L.J.F. and Peletier L.A. (1960): *A Mechanical. Hall Effect.*– Appl. Sci. Res., vol.8B, pp.259.

[5] Sato H. (1961): *The Hall effect in the viscous flow of ionized gas between parallel plates under transverse magnetic field.*– J. Phys. Soc. Japan, vol.16, No.7, pp.1427-1433.

[6] Tani I. (1962): *Steady flow of conducting fluids in channels under transverse magnetic fields with consideration of Hall effect.*– J. Aerospace Sci., vol.29, pp.297.

[7] Pop I. (1971): *The effect of Hall current on hydromagnetic flow near accelerated plate.*– J. Math. Phys. Sci., vol.5, pp.375-379.

[8] Cramer Kenneth R. and Pai Shih-I. (1973): *Magneto fluid Dynamics for Engineers and Applied Physicists.*– McGraw-Hill Company, p.347.

[9] Shercliff J.A. (1979): *Thermoelectric magnetohydrodynamics.*–J. Fluid Mechanics, vol.91, No.2, pp.231-251.

[10] Sharma R.C. and Neela Rani (1988): *Hall effects of thermo-solute instability of a plasma.*– Indian J. Pure Appl. Math, vol.19, No.2, pp.202-207.

[11] Niranjan S.S., Soundalgekar V.M. and Takhar H.S. (1990): *Free convection effects on HMD horizontal channel flow with Hall currents.*– Plasma Sci. IEEE Trans, vol.18, No.2, pp.177-183.

[12] LingaRaju T. and Ramana Rao V.V. (1992): *Hall effect in the viscous flow of an ionized gas between two parallel walls under transverse magnetic field in a rotating system.*– Acta Physica Hungarica, vol.72, No.1, pp.23-45.

[13] LingaRaju T. and Ramana Rao V.V.(1993): *Hall effects on temperature distribution in a rotating ionized hydromagnetic flow between parallel walls.*– Int. J. Engg. Sci., vol.31, No.7, pp.1073-1091.

[14] Attia H.A. (1998): *Hall current effects on the velocity and temperature fields of an unsteady Hartmann flow.*– Can. J. Phys, vol.76, No.9, pp.739-746.

[15] Aboeldahab E.M. and Elbarbary E.M.E. (2001): *Hall current effect on magnetohydrodynamic free convection flow past a semi-infinite vertical plate with mass transfer.*– Int. J. Engg. Sci., vol.39, pp.1641-1652.

[16] Singh J.K., Begum S.G. and Seth G.S. (2018): *Influence of Hall current and wall conductivity on hydromagnetic mixed convective flow in a rotating Darcian channel.*– Physics of Fluids, vol.30, No.11, p.12.

[17] Milica N., Zivojin S., Jelena P. and Milos K. (2020): *Unsteady fluid flow and heat transfer through a porous medium in a horizontal channel with an inclined magnetic field.*– Transactions of FAMENA, vol.44, No.4, pp.31-46. DOI: https://doi.org/10.21278/TOF.444014420.

[18] Jitendra K.S. and Suneetha K. (2021): *Energy dissipation and Hall effect on MHD convective flow of nanofluid within an asymmetric channel with arbitrary wall thickness and conductance.*- The European Physical Journal Plus,vol.136, article number 1074, DOI:https://doi.org/10.1140/epjp/s13360-021-02022-6.

[19] Jitendra K.S., Suneetha K. and Gauri S.S. (2022): *Scrutiny of induced magnetic field and Hall current impacts on transient hydromagnetic nano fluid flow within two vertical alternative magnetized surfaces.*– Proceedings of the

Institution of Mechanical Engineers, Part E: Journal of Process Mechanical Engg.,vol.237, No.4.pp.1595-1606. DOI:https://doi.org/10.1177/095440892211192.

[20] Jitendra K.S. and Vishwanath S. (2022): *Hall and induced magnetic field effects on MHD buoyancy-driven flow of WaltersB fluid over a magnetised convectively heated inclined surface.*– International Journal of Ambient Energy, vol.43, No.1, pp.4444-4453. DOI:https://doi.org/10.1080/01430750.2021.1909652.

[21] Jitendra K.S., Gauri S.S. and Syed M.H. (2023): *Thermal performance of hydromagnetic nanofluid flow within an asymmetric channel with arbitrarily conductive walls filled with Darcy-Brinkman porous medium.*– Journal of Magnetism and Magnetic Materials, vol.582, article number 171034, DOI:https://doi.org/10.1016/j.jmmm.2023.171034.

[22] Jitendra K.S., Hanumantha, Suneetha K. and Syed M.H. (2023): *Exploration of heat and mass transport in oscillatory hydromagnetic nano fluid flow within two verticals alternatively conducting surfaces.*– ZAMM,vol.103, No.12, pp. 1-20, DOI:https://doi.org/10.1002/zamm.202300216.

[23] Thatcher (1973): *Electromagnetic Flow Meters For Liquid Metals, In Modern Development In Flow Measurement.*– Clayton, C.G. (ed). London Peter Peregrinus Ltd., pp. 359-380.

[24] Chwla T.C. and Ishii M. (1980): *Two-fluid model of two-phase flow in a pin bundle of a nuclear reactor.*– Int. J. Heat Mass Transfer, vol.23, pp.991-1001.

[25] Dunn P.F. (1980): *Single-phase and two-phase magnetohydrodynamic pipe flow.*– Int. Journal of Heat and Mass Transfer, vol.23, pp.373.

[26] Dobran F. (1981): *On the consistency conditions of averaging operators in 2-phase flow models and on the formulation of magnetohydrodynamic 2-phase flow.*– Int. J. Eng. vol.19,No.10, pp.1353-1368.

[27] Mitra P. (1982): *Unsteady flow of two electrically conducting fluids between two rigid parallel plates.*– Bulletin of the Calcutta Mathematical Society, vol.74, pp.87-95.

[28] Lohrasbi J. and SahaiV. (1988): *Magnetohydrodynamic heat transfer in two phase flow between parallel plates.*– Appl. Sci. Res., vol.45, pp.53-66.

[29] Setayesh A. and Sahai V. (1990): *Heat transfer in developing magnetohydrodynamic Poiseuille flow and variable transport properties.*– Int. J. Heat Mass Transfer, vol.33, No.8,pp.1711.

[30] Malashetty M.S. and LeelaV. (1992): *Magnetohydrodynamic heat transfer in two phase flow.*– Int. J. of Engg. Sci., vol.30, pp.371-377.

[31] Chamkha A.J. (2000): *Unsteady laminar hydromagnetic fluid-particle flow and heat transfer in channels and circular pipes.*– Int. J. of Heat and Fluid Flow, vol.21, pp.740-746.

[32] Umavathi J.C., Chamkha A.J., Mateen A. and Kumar J.P. (2008): *Unsteady magneto-hydrodynamic two fluid flow and heat transfer in a horizontal channel.*– Heat and Technology, vol.26, No.2, pp.121-133.

[33] Tsuyoshi Inoue and InutsukaShu-Ichiro (2008): *Two-fluid MHD simulations of converging Hi flows in the interstellar medium I:Methodology and basic results.*– The Astr. Phys. J., vol.687, pp.303-310.

[34] Hussameddine S.K., Martin J.M. and Sang W.J. (2008): *Analytical prediction of flow field in magnetohydrodynamic based micro fluidic devices.*– J. of Fluids Engg, vol.130,No.9, pp.6-10.

[35] Srivastava K.M. (2009): *Effect of Hall current on the instability of an anisotropic plasma.*–Jet. J. Plasma Phys., vol.12, No.1, pp.33-43.

[36] Stamenkovic M.Z., Nikodjevic D.D, Blagojevic B.D. and Savic S. (2010): *MHD flow and heat transfer of two immiscible fluids between moving plates.*– Transactions of the Canadian Society for Mechanical Engg., vol.34, No.3-4, pp.351-372.

[37] Stamenkovic Ź.M., Nikodijevic D.D., Kocic M.M. and Nikodijevic J.D. (2012): *MHD flow and heat transfer of two immiscible fluids with induced magnetic field.*– Thermal Science: Int. Scientific Journal, vol.16, No.2, pp.323-336.

[38] LingaRaju T. and Valli M. (2014): *MHD two-layered unsteady fluid flow and heat transfer through a horizontal channel between parallel plates in a rotating system.*– Int. J. Appl. Mech. and Engg., vol.19, No.1, pp.97-121.https://doi.org/10.2478/ijame-2014-0008.

[39] Selimli S., Resebli Z. and Arcakhoglu E. (2015): *Combined effects of magnetic and electric field on hydrodynamic and thermo-physical parameters of magneto-viscous fluid flow.*– Int. J. Heat Mass Trans., vol.86, pp.426-432.

[40] Kalra G.L., KathuriaS.N., Hosking R.J. and Lister G.G. (1970): *Effect of Hall current and resistivity on the stability of a gas-liquid system.*– J. Plasma Phys., vol.4, No.3, pp.451-469. Doi:10.1017/S0022377800005158.

[41] Hyun S. and Kennel C.F. (2009): *Small amplitude waves in a hot relativistic two-fluid plasma.*– J. Plasma Phy., vol.20, No.2, pp.281-287.

[42] Sharma P.R. and Sharma Kalpana (2014): *Unsteady MHD two-fluid flow and heat transfer through a horizontal channel.*– Int. J. of Engineering Science Invention Research and Development, vol.1, No.3, pp.65-72.

[43] Joseph K.M., Peter A., Asie P.E. and Usman S. (2015): *The unsteady MHD free convective two immiscible fluid flows in a horizontal channel with heat and mass transfer.*– Int. J. of Mathematics and Computer Research, vol.3, No.5, pp.954-972.

[44] Sivakamini L. and Govindarajan A. (2019): *Unsteady MHD flow of two immiscible fluids under chemical reaction in a horizontal channel.*– AIP conference proceedings 2112.020157 https://doi.org/10.1063/1.5112342, published online: 24 June 2019.

[45] Gireesha B.J., Mahantesh B., Thammanna G.T. and Sampath Kumar P.B.(2018): *Hall effects on dusty nanofluid two-phase transient flow past a stretching sheet using KVL model.*– Journal of Molecular Liquids, vol.256, pp.139-147. https://doi.org/10.1016/j.molliq.2018.01.186.

[46] Linga Raju T. (2019): *MHD heat transfer two-ionized fluids flow between parallel plates with Hall currents.*– Journal of Results in Engineering, Elsevier Publication. vol.4, p.100043, https://doi.org/10.1016/j.rineng.2019.100043.

[47] LingaRaju T. (2021): *Electro-magneto hydrodynamic two fluid flow of ionized-gases with Hall and rotation effects.*– Int. J. Appl. Mech., vol.26, No.4, pp.128-144, DOI: 10.2478/ijame-2021-0054.

[48] Linga Raju T. and GowriSankaraRao V. (2021): *Effect of Hall current on unsteady magneto hydrodynamic two-ionized fluid flow and heat transfer in a channel.*– Int. J. of Applied Mechanics and Engg., vol.26, No.2, pp. 84-106.https://doi.org/10.2478/ijame-2021-0021.

[49] Linga Raju T. and GowriSankaraRao V. (2023): *An unsteady electro-magnetohydrodynamic two-liquid plasma flow along a channel of insulating porous plates with Hall currents.*– Int. J. of Applied Mechanics and Engg., vol.28, No.2, pp.90-112, DOI: 10.59441/ijame/168933.

[50] Linga Raju T. and Valli Naga M. (2023): *Effect of hall currents on the MHD two-layered plasma heat transfer flow via a channel of porous plates.*– Journal of Engineering Physics and Thermo Physics.,vol.96, No.5. pp.1-12, DOI 10.1007/s10891-023-02794-x.

[51] Linga Raju T. and VenkatRao B. (2022): *Unsteady electro-magneto hydrodynamic flow and heat transfer of two ionized fluids in a rotating system with Hall currents.*– Int. J. of Applied Mechanics and Engg., vol.27, No.1. pp.125-145, DOI: 10.2478/ijame-2022-0009.

[52] Linga Raju T. and VenkatRao B. (2022): *The Hall effect on MHD 2-fluid unsteady heat transfer flow of plasma in a rotating system via a straight channel between conducting plates.*– Int. J. of Applied Mechanics and Engg.,vol.27, No.3. pp.137-162, DOI: 10.2478/ijame-2022-0041.

[53] LingaRaju T. and Satish P. (2023): *Hall and rotation effects on magnetohydrodynamics two fluids slip flow of ionized gases via parallel conduit.*– Heat Transfer, vol.52, No.7. pp.137-162, DOI:10.1002/htj.22909.

[54] Linga Raju T. and Satish P. (2023): *Slip regime MHD 2-liquid plasma heat transfer flow with hall currents between parallel plates.*– Int. J. Appl. Mech. and Engg., vol.28, No.3. pp.65-85, https://doi.org/10.59441/ijame/172898.

[55] Spitzer L. Jr. (1956): *Physics of Fully Ionized Gases.*– Inter science Publishers, N. Y.